Naphthalimide-NHC complexes: Synthesis and properties in catalytic, biological and photophysical applications

Liza Roos, Frederick P. Malan* and Marilé Landman*
Department of Chemistry, University of Pretoria, Hatfield, Pretoria, South Africa, 0002
E-mail: marile.landman@up.ac.za; frikkie.malan@up.ac.za

Highlights

•A comprehensive review on naphthalimide-containing N-heterocyclic carbene complexes.

•Emphasis on imidazolinylidenes and (benz)imidazolylidene ligands as NHC frameworks.

•Catalysis, biological studies and luminescence discussed employing these complexes.

Abstract

The following review provides an account of all 82 N-heterocyclic carbene metal complexes containing a naphthalimide-NHC moiety, incorporating either an imidazolylidene, imidazolinylidene or benzimidazolylidene ligand, reported in literature. Only three of these are biscarbene complexes. Naphthalimide-NHC complexes constitute a very successful class of compounds that has been applied across many fields, thus providing a focal point of coinciding interest that may appeal to a wide audience and incite future work. Herein, the complexes are divided among those with the naphthalimide moiety tethered *via* a (benz)imidazol(in)ylidene N-atom and those where it is bonded to the NHC backbone, since the electronic properties and conformations of the two classes vary considerably. These complexes are interesting target molecules that rely on common to more advanced synthetic methods for preparation, including post-synthetic modification in some instances. Due to their bulkiness, these complexes may also exhibit notable conformations in the solid state, with π-π stacking interactions contributing to their fascinating properties. Catalytic applications for this class of complexes are limited in literature and include only the Larock heteroannulation reaction and Suzuki-Miyaura coupling reaction. Pd(II) complexes were primarily studied as catalysts for these reactions. Au(I), Cu(I), Ag(I), Rh(I) and Ru(II) complexes were applied in a biological context, with bis-naphthalimide Ag(I) and bis-NHC Au(I) complexes showing the greatest activity against cancerous colorectal (HT-29), breast (MCF-7) or lung (A549) cells. The naphthalene rings of the naphthalimide moiety in the complexes were responsible for π-π stacking interactions and binding of complexes to DNA through intercalation. Rh(I), Ru(II) and Ag(I) complexes successfully

inhibited gram positive bacterial strains. In addition, Au(I), Cu(I), Ag(I), Rh(I), Ir(I) and Ir(III) complexes exhibited photoluminescent properties, emitting in red, blue-green or blue regions with either phosphorescence or fluorescence lifetimes. The unique properties of naphthalimide-NHC complexes allowed for the theranostic application in selected anticancer studies, which has been illustrated by imaging of cytotoxic luminescent complexes. Integration of the photophysical properties with catalytic processes, in photocatalysis or in additional biological applications e.g. photodynamic therapy, is envisaged for these naphthalimide-containing complexes in future endeavours.

Graphical abstract

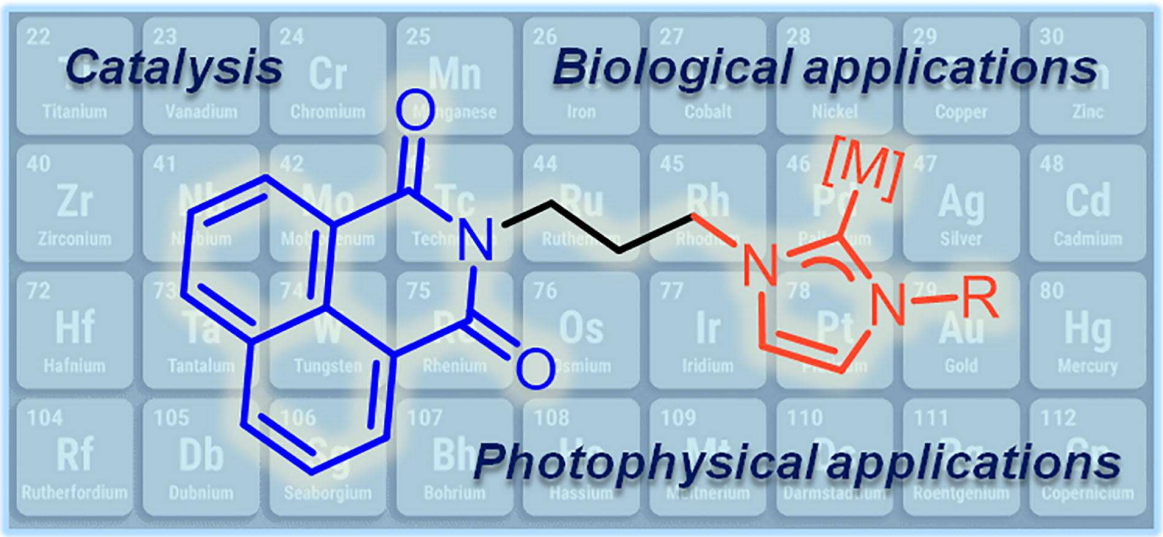

Keywords: naphthalimide, N-heterocyclic carbene, Larock heteroannulation, Suzuki-Miyaura, anticancer, antibacterial, fungicidal, photoluminescence

Contents

Abbreviations: bipy, 2,2'-bipyridine; BODIPY, boron dipyrromethene; BSA, bovine serum albumin; CAAC, cyclic alkyl amino carbenes; cat, catalyst; CD, circular dichroism; COX, cyclooxygenase; DFT, density functional theory; DIPEA, N,N-diisopropylethylamine; DMAP, 4-dimethylaminopyridine; DSSC, dye-sensitised solar cell; DUB, deubiquitinase; FLIM, fluorescence lifetime imaging microscopy; FRET, fluorescence resonance energy transfer; GR, glutathione reductase; HOMO, highest occupied molecular orbital; ICT, intraligand charge transfer; LC, ligand centred; LUMO, lowest unoccupied molecular orbital; MAPK, mitogen-activated protein kinases; MLCT, metal-to-ligand charge transfer; MMRP, mitochondrial membrane redox potential; mtROS, mitochondrial reactive oxygen species; NBO, natural bond order; NHC, N-heterocyclic carbene; OLED, organic light emitting diode; PDT, photodynamic therapy; py, pyridine; SCXRD, single crystal X-ray diffraction; SD, standard deviation; SEM, standard error of the mean; TBAB, tetrabutylammonium bromide; TBAF, tetra-n-butylammonium fluoride; TEA, triethylamine; TrxR, thioredoxin reductase; TUNEL, terminal deoxynucleotidyl transferase dUTP nick end labelling; tpy, terpyridine.

1. Introduction

The basic 1,8-naphthalimide moiety, or 1H-benz[de]isoquinoline-1,3(2H)-dione, is a well-known, stable fluorophore that can be described as a polycyclic imide with π-deficient naphthalene rings [1,2]. Since the imide groups are bonded at the *peri*-positions of the naphthalene rings, 1,8-naphthalimides belong to a class known as rylenes [3]. A review article by Kamal *et al.*, published in 2013, provided an impressive account of all the patents that have been registered between 2006 and 2011 for naphthalimides applied as therapeutic agents [4]. The 1,8-naphthalimide moiety has frequently been incorporated into molecular design across a number of research fields, which include anticancer medicines and fluorescent probes, that may or may not contain transition metals [5-7]. Fig. 1 depicts a few selected examples to illustrate its vast occurrence.

In a study by Qian *et al.* three fluorescent probes with maleimide moieties attached at different positions, were synthesised and studied for the detection of harmful thiols [8]. It was shown

that the spacer between the fluorophore and the maleimide moiety had an important influence on the fluorescent response toward thiols [8]. Example 1 (Fig. 1) depicts the most selective of their three probes. Example 2 (Fig. 1) represents one of a series of compounds studied by Carlotti *et al.,* which incorporated the naphthalimide moiety into multichromophoric molecules, with the naphthalimide attached at different positions of the boron dipyrromethene (BODIPY) fragments [9]. These compounds can be employed as fluorescent probes in bio-imaging and in the conversion of solar energy into electricity [9]. In a similar fashion, Liu *et al.* combined naphthalimide and hydrazine carbothiourea or hydrazine carboxylate moieties to synthesise two probes for anion-induced detection of CO_2, of which one is given as example 3 (Fig. 1) [10].

Several organic compounds, which contain both an azole and a naphthalimide moiety in the molecule, have been studied in literature. Azoles are a prominent class of compounds that often exhibit appreciable antibacterial and fungicidal properties due to favourable interactions with biomolecular targets [11,12]. Examples containing (benz)imidazole [11-15] and/or 1,2,4-triazole [11,12,16], that in some cases have also been converted to corresponding azolium salts [11,12,14], have been investigated for anticancer [12,13], antibacterial [11,12], fungicidal [11,12], theranostic [15], photophysical [14] and anion sensing applications [16]. One example of such a compound is shown in Fig. 1 (example 4) [11].

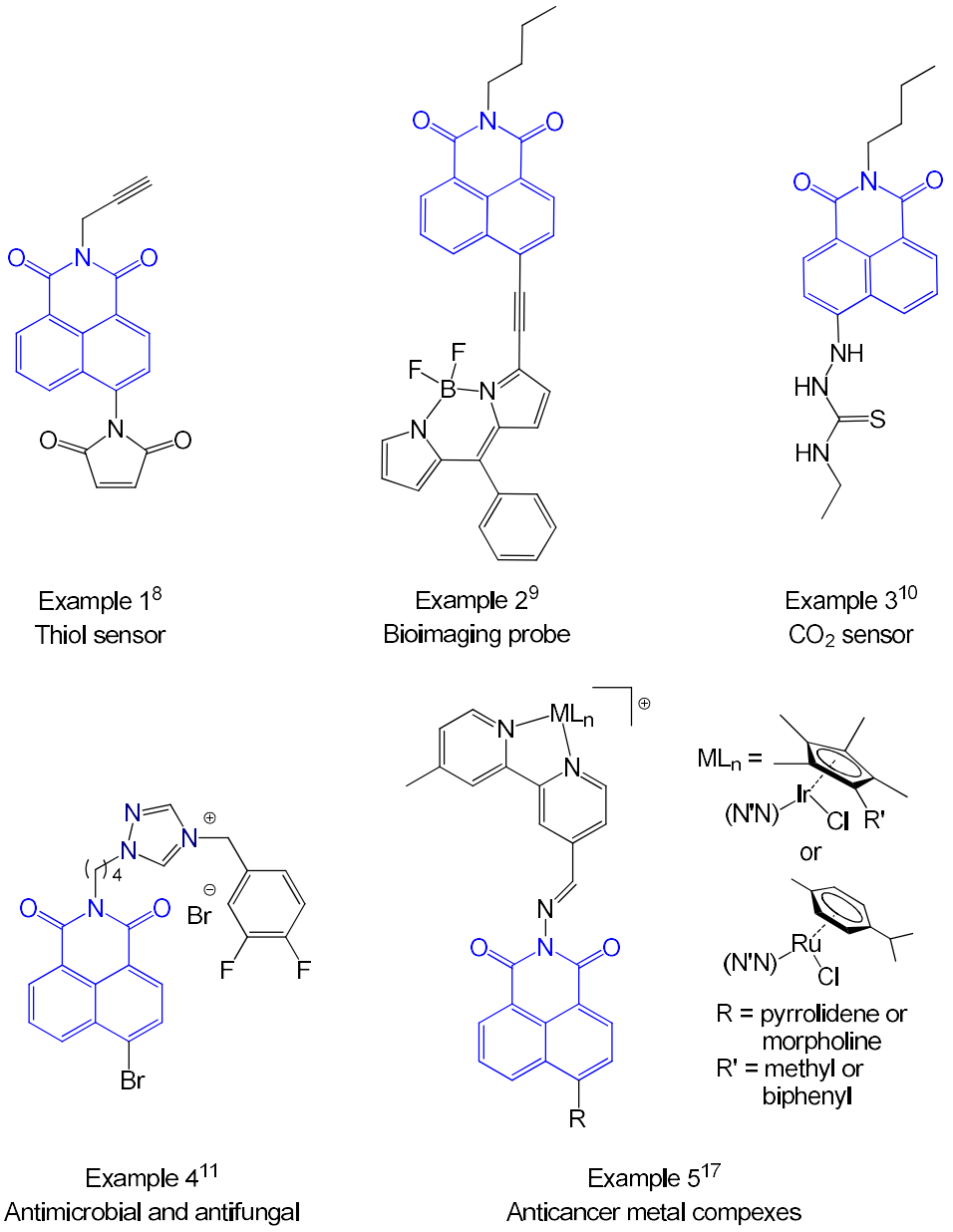

Fig. 1. Naphthalimide-containing compounds with distinct applications.

Ma *et al.* synthesised five non-NHC, N,N'-coordinated ruthenium and iridium complexes with varied substituents at the *para*-position of the naphthalene rings, shown in example 5 (Fig. 1) [17]. These complexes showed excellent anticancer activity and their fluorescent properties allowed the visualisation and study of the drug's mechanism of action [17]. The ability of many azolium salts to act as NHC ligands is still unexplored. For transition metal complexes, only imidazolylidene, imidazolinylidene or benzimidazolylidene NHC ligands, containing the naphthalimide moiety either in the tether or bonded to the NHC backbone, exist in literature.

NHC ligands in general have systematically replaced phosphines as strong σ-donating ligands that stabilise most transition metals in a variety of oxidation states [18]. In some cases it even allows for the isolation of previously inaccessible high oxidation state metal species [19]. In terms of ligand tunability with regards to steric bulk, flexibility, electronic properties, as well as the possibility to include a plethora of function-specific functional groups embedded within the ligand [18], NHCs have developed to such an extent to out-perform the possibilities that most commercial and custom phosphines may offer. Incorporating the naphthalimide moiety into the NHC scaffold not only creates a unique steric and electronic environment that can be probed during catalysis, but the aromatic rings promote non-innocent, bifunctional behaviour through π-π stacking interactions. Additionally, these π-π stacking interactions posit non-covalent interactions with DNA, which realise the possible biological applications of these complexes. Since the naphthalimide moiety is a well-known chromophore, these complexes may also have appreciable photophysical properties. This class of compounds thus plays into two of the major trends currently of interest in metal NHC chemistry: being non-innocent or SMART [20], with sparse literature reports on bifunctional behaviour through π-π stacking interactions [21], and diversifying applications [22] beyond catalysis. These NHC-naphthalimide ligands therefore simultaneously provide a multitude of potential catalytic, biological, and photophysical applications that render metal complexes thereof multi-functional, as opposed to related bulky phosphine counterparts. This is a highly desirable property especially from an economical point of view. Despite the advantages the NHC-naphthalimide family of compounds hold, reports on the corresponding complexes and their applications remain relatively scarce, especially when compared to commercially available NHC and phosphine ligands and corresponding complexes. The few facile synthetic routes to these NHC-naphthalimide (pre-)ligands are believed to be responsible for the impediment in terms of ligand development.

Review articles that cover a specific subset of naphthalimide-NHC complexes are available, with naphthalimide-containing compounds discussed in the context of either anticancer [23-26] or photophysical applications [27,28]. We have identified naphthalimide-NHC complexes as a unique class of interesting compounds among these reports, especially when the potential overlap with catalytic applications was also considered. All naphthalimide-containing NHC complexes found in literature contain the naphthalimide moiety in the NHC scaffold and are complexed to coinage- or platinum-group metals. This review provides a comprehensive account of all 82 naphthalimide-NHC complexes described to date, in addition to providing

details of their synthesis, characterisation and applications. The complexes covered in this review are divided into two categories: those containing the naphthalimide moiety tethered *via* a (benz)imidazol(in)ylidene N-atom (Fig. 2) and those with it bonded to the NHC backbone (Fig. 3). In these figures, complexes are classified among fourteen scaffolds (**A**-**N**) that are arranged according to their application fields. It is illustrated here for the first time that naphthalimide-NHC complexes feature across multiple research fields, contextualising the terms 'catalyst', 'chromophore' and 'intercalate'. Overlap between fields shows how complexes with the same basic scaffold (e.g. **A** and **H**) have been applied in two distinct fields (catalysis and biological or luminescence and conformational studies) or how distinct fields (biological and luminescence) were hybridised for subsequent specialised applications (e.g. **E**).

The complexes are listed in such a way that the potential to hybridise and 'overlap' the application fields further is especially exemplified. Naphthalimide-NHC complexes have thus far been applied for cellular imaging applications (which combines luminescent and biological application fields). The undeniable versatility of naphthalimide-NHC complexes, however makes them viable candidates for photodynamic therapy (PDT) or photocatalysis which would involve integrating their photophysical and biological or catalytic properties, respectively. Compounds appropriate for PDT is highly desirable considering the non-invasive nature and potential of PDTs to act against multi-drug resistant cancers [29]. Additionally, recent advances in PDT focus on targeting specific organelles which coincides with the cellular imaging studies that have been done for some of the naphthalimide-NHC complexes [29].

2. Synthesis and Characterisation

The synthesis and characterisation of the naphthalimide-containing complexes are discussed with reference to Fig. 2 and 3, which divide them into complexes with the naphthalimide moiety either tethered to the NHC scaffold *via* an N-atom (complexes **1**-**24**, Fig. 2) or as part of the NHC backbone (complexes **25**-**29**, Fig. 3). It is common to distinguish between complexes containing imidazolylidene and benzimidazolylidene derivatives, as the backbone of NHCs plays an important role in mesoionic coordination [30]. In addition, benzimidazole complexes as a distinct class of compounds, known as 'annellated NHCs' [31], often impact the solubility of complexes significantly. The position of the naphthalimide moiety *i.e.* in the tether or in the backbone of the NHC ligand is an apparent structural distinction also prudently

considered by Panyam *et al.* [32,33] and Dangalov *et al.* [34-37], who synthesised and studied complexes **1**, **6-8**, **25** and **24**, **26-29**, respectively.

The azolium salts of the respective complexes were synthesised by general consideration of two main strategies that involved either an initial condensation or substitution reaction, followed by N-quaternisation (*vide infra*). For the azolium salts of complexes **9-12** [38], **13a-h** [39], **18-20** [40,41] and **26-29** [5,14,35,37] alternative methods (*vide infra*) were followed. Numbers used are those of the final complexes presented in Fig. 2 and 3 that were subsequently synthesised from the precursors.

The first step in the synthesis of many of the azolium salts involved the modification of 4-halo-1,8-naphthalic anhydride (Scheme 1). In this step (Scheme 1), 4-halo-1,8-naphthalic anhydride was converted to either 4-ethylthio-1,8-naphthalic anhydride (**2d** [42], **3d-f** [1,43], **4d-f** [1,43], **9b-12b** [38]) or 4-halo-N-alkyl-naphthalimide (**13-15** [39,41], **16-17** [44], **21-22** [45-47], **23** [47], **24** [34]). Further modification of the precursor of **16b** and **17b** required nucleophilic aromatic substitution with 2-aminoethanol to yield the intermediate alcohol (step (d) i. in Scheme 1) [44]. For **18**, 4-bromo-N-hydroxyethyl-naphthalimide underwent nucleophilic aromatic substitution by reaction with morpholine in the presence of NEt_3 (route e) or a palladium catalyst (route f) (Scheme 1) [48]. The latter method is termed a Buchwald-Hartwig cross-coupling reaction and for both routes (e) and (f) in Scheme 1, the naphthalimide derivative was obtained in 60% yield [48]. Yu *et al.* also reported on a method whereby aromatic substitution of bromine with morpholine occurred prior to the condensation step involving ethanolamine [49]. Three preceding steps were involved in the formation of **26-29**'s precursors (Scheme 1), whereby 4-bromo-1,8-naphthalic anhydride was converted to 4-bromo-3-nitro-1,8-naphthalic anhydride followed by conversion to 4-amino-3-nitro-N-alkyl-naphthalimide and finally to 3,4-diamino-N-alkyl-naphthalimide [5,14,35,36].

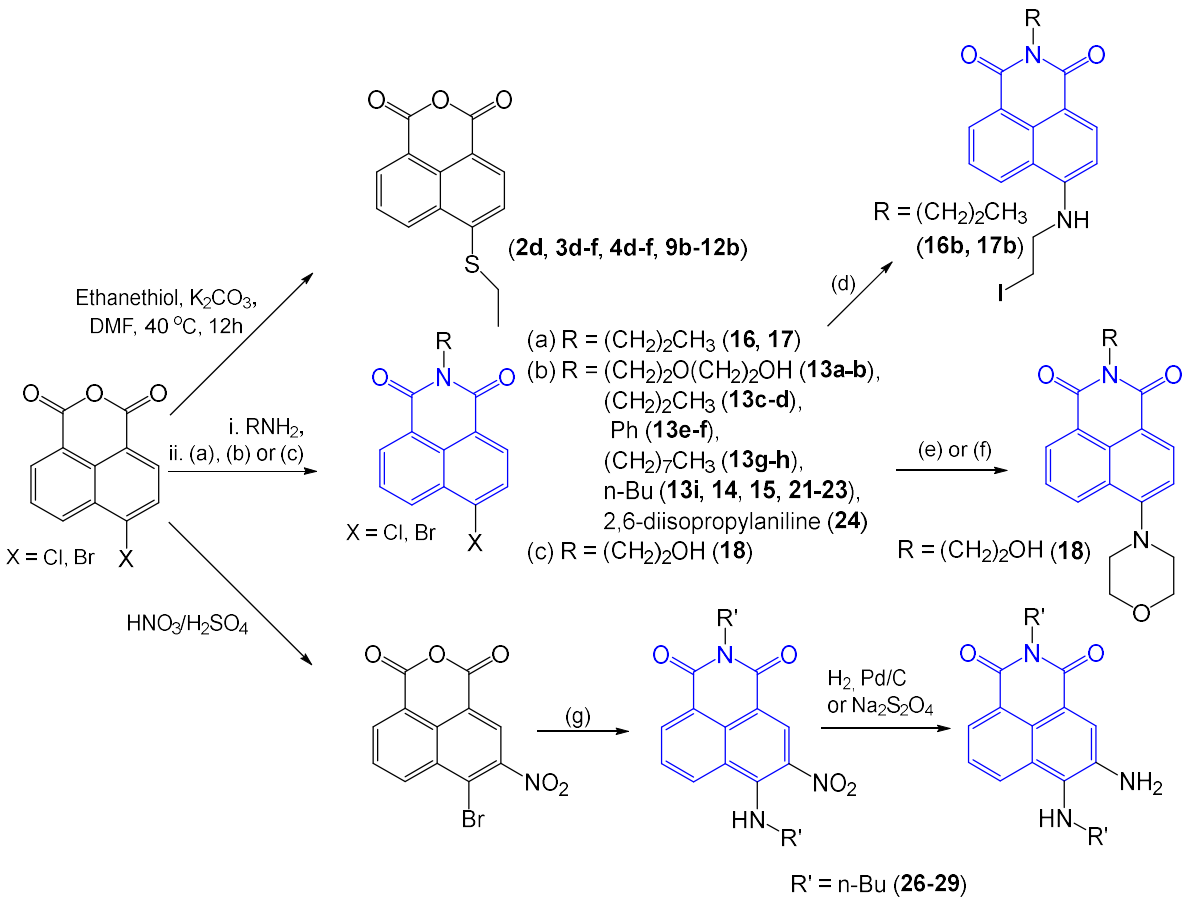

Scheme 1. Conversion of 4-halo-1,8-naphthalic anhydride to appropriate 1,8-naphthalic anhydride/naphthalimide derivatives required for the synthesis of azolium salts (*vide infra*). Bold numbers are those of the final complexes presented in Fig. 2 and 3 that were subsequently synthesised from these derivatives. Reaction labels (a), (b) and (c) as well as (e) and (f) refer to three/two sets of reaction conditions that were followed in each case, respectively. Reaction conditions: (a) TEA, EtOH, reflux overnight; (b) CH_3COOH, reflux; (c) EtOH, MW (100 °C), 45 min; (d) i. TEA, 2-aminoethanol, DMSO, 120 °C, 96h; ii. THF, PPh_3, imidazole, I_2, RT, 15 min followed by stirring at 65 °C, 3h; (e) Morpholine, NEt_3, EtOH, MW (100 °C), 4h; (f) Morpholine, 4 mol % $Pd_2(dba)_3 \cdot CHCl_3$, 4 mol % Xantphos, 3 eq. Cs_2CO_3, toluene, 60 °C, 48h (g) i. $R'NH_2$, Δ, 24h, cool RT, ii. $CH_3CH_2CO_2H$, 140 °C, 24h.

2.1 N-tethered naphthalimide complexes

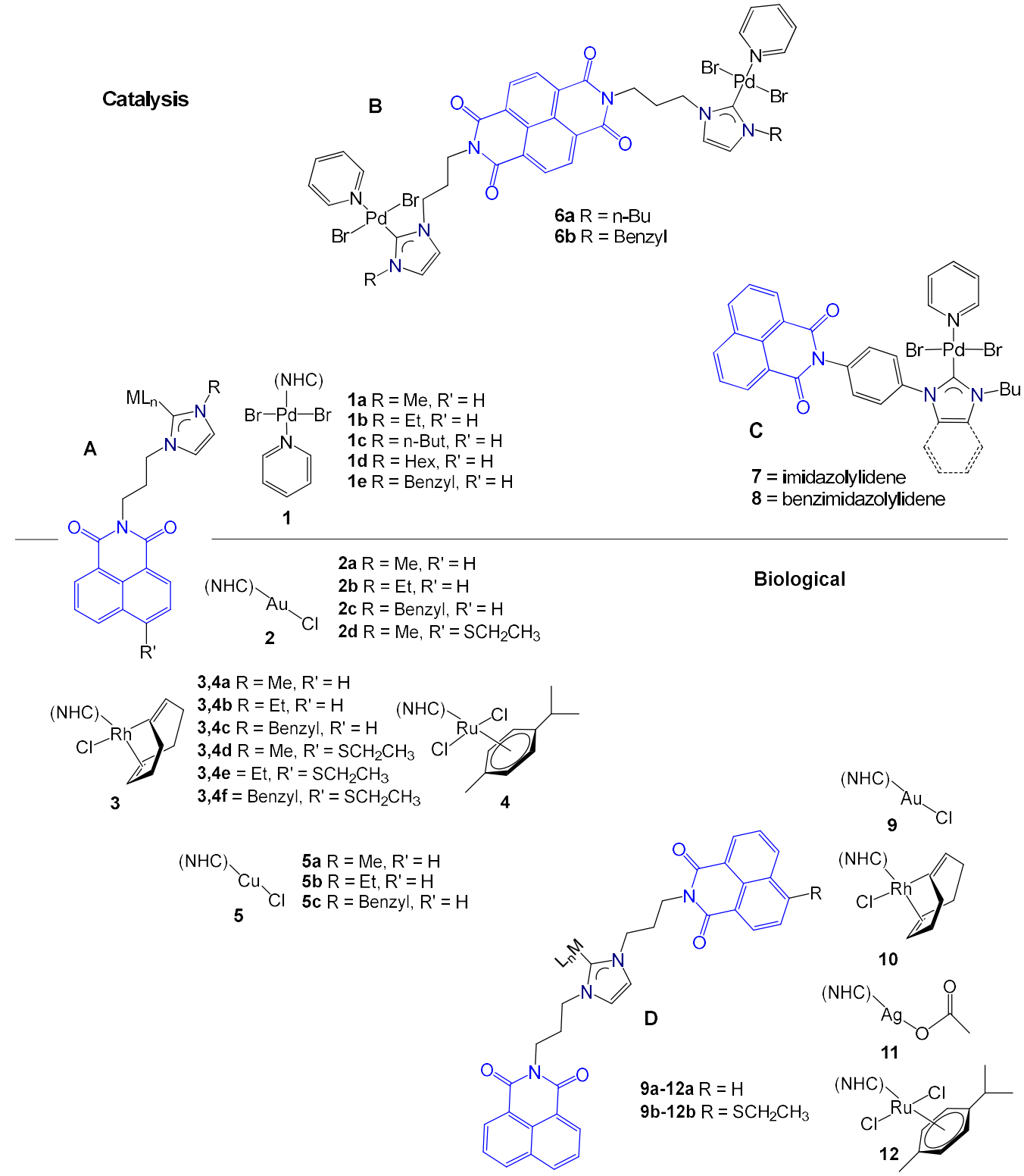

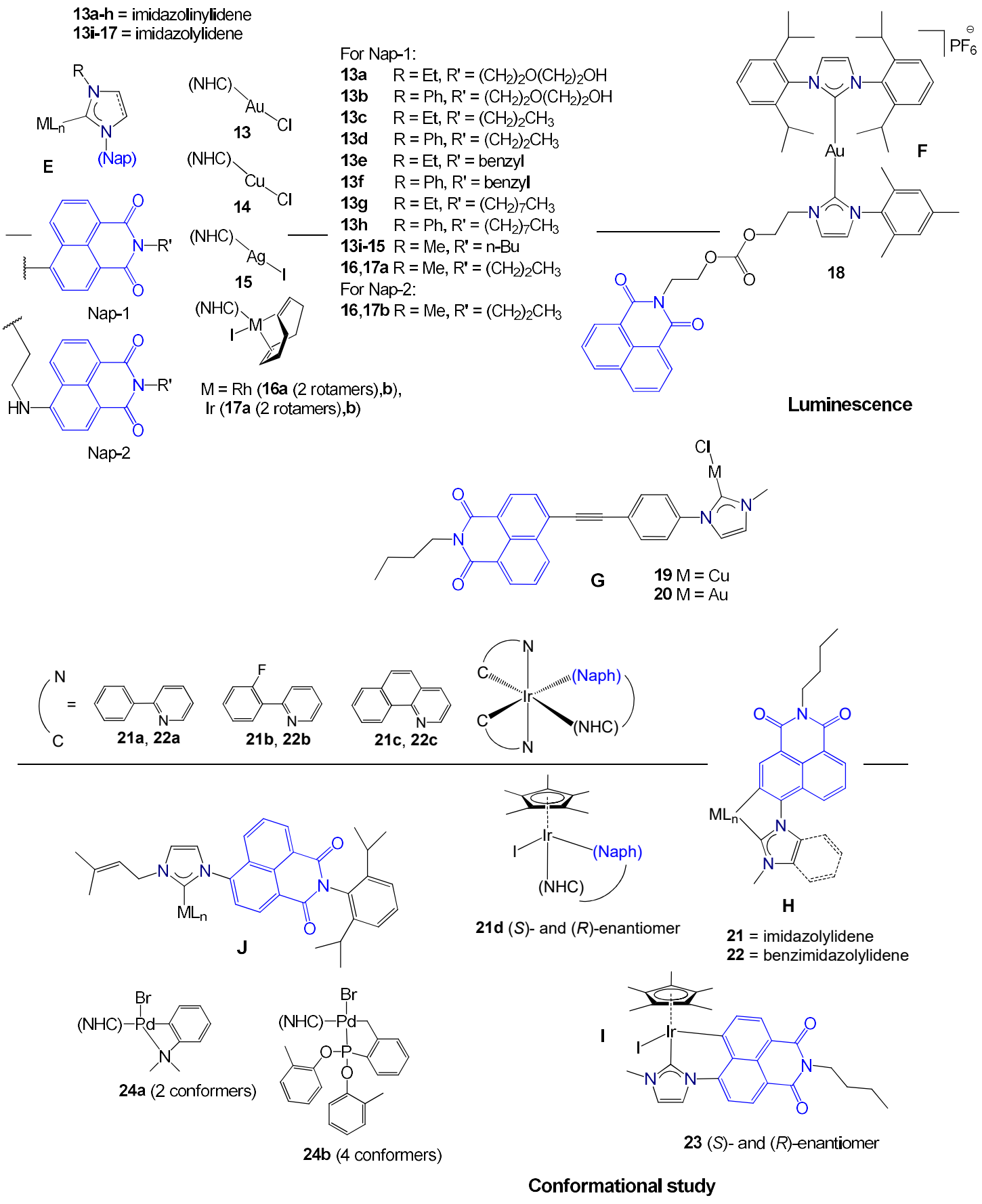

Fig. 2. Naphthalimide-NHC complexes with the naphthalimide moiety tethered *via* a(n) (benz)imidazol(in)ylidene N-atom, classified according to their application and grouped into nine basic scaffolds (**A-I**). Overlap between application fields is indicated by bridging structures.

Azolium salts of complexes with the naphthalimide moiety tethered *via* the (benz)imidazolylidene N-atom, as presented by scaffolds **A-D** (Fig. 2), were synthesised using amino-containing imidazole-heterocycles in an initial condensation step, achieved by refluxing with the respective 1,8-naphthalic anhydride derivative in toluene [32], EtOAc [1,38,42,50] or EtOH [33] for 5-36h (Scheme 2). Additionally, for **1** [32], **7** [33] and **8** [33], triethylamine was added. The initial condensation step involved 1-(3-aminopropylimidazole) (**1-6** [1,32,42,50], **9-12** [38]), 4-(1H-imidazol-1-yl)aniline (**7** [33]) or 4-(1H-benzimidazol-1-yl)aniline (**8** [33]) and 1,8-naphthalic anhydride (**1** [32], **2-5a-c** [42,50], **7** [33], **8** [33], **9a-12a** [38]), 4-ethylthio-1,8-naphthalic anhydride (**2d** [42], **3-4d-f** [1]) or 1,4,5,8-naphthalene tetracarboxylic dianhydride (**6** [32]). For **A-D** (complexes **1-12**), the subsequent quaternisation step generally involved refluxing of the functionalised imidazole with the respective alkyl halide in CH_3CN or as for **2** [42], in toluene at 90 °C-110 °C for 2-72h to give the corresponding compounds in good to high yields (55-98%). In Table 1 the yield values specific to each azolium salt are presented.

Introduction of the naphthalimide moiety during an initial substitution step was mainly considered for complexes tethered *via* a C-atom in the naphthalene rings, as presented by scaffolds **E** and **G-I** (Fig. 2). For **16a** and **17a** [44], **13i-15** [41], **21** [45-47], **22** [46], **23** [47] and **24** [34] this generally involved reacting imidazole or benzimidazole with a 4-halo-1,8-naphthalimide derivative (Scheme 2). In the case of **13i-15** [41], **16a**-**17a** [44], 2**1** [45-47], **22** [46] and **23** [47], the reaction took place at approximately 110 °C in DMSO with K_2CO_3 whereas for **24** [34,51] at 100 °C in DMF in the reaction of Cs_2CO_3, CuI and (*S*)-(N-benzylpyrrolidin-2-yl)-2-methylimidazole (a proline-based ligand). Quaternisation for **E** and **G-I** (complexes **13-16a**, **17a** and **19-23**) was achieved similar to what was reported for scaffolds **A-D**, albeit at lower reaction temperatures, with yields ranging from 45-85% (Table 1). For complexes **16b** and **17b** the naphthalimide moiety was introduced during the quaternisation step to yield the precursor imidazolium salt. The substitution occurred between the iodoethylamino tether of the naphthalimide moiety and 1-methylimidazole when reacted together at 65 °C in THF for 72h [44].

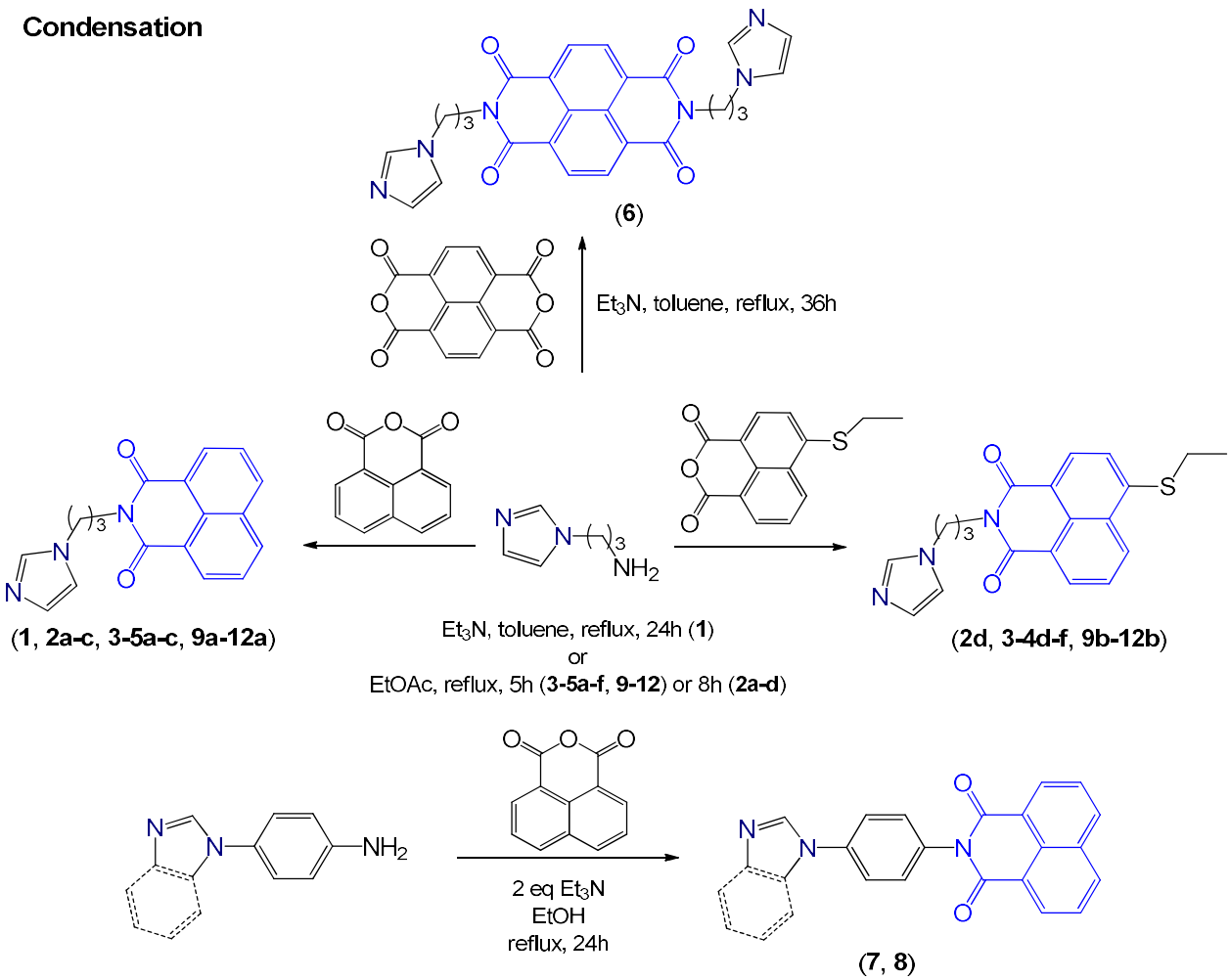

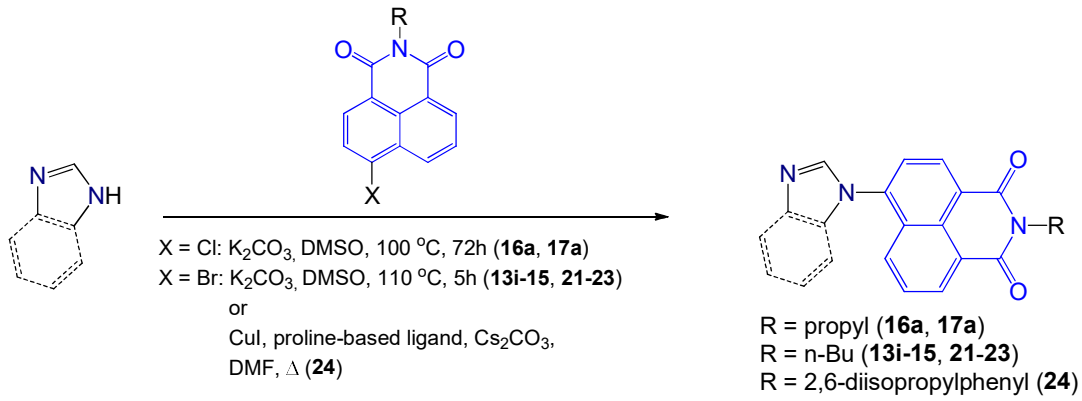

Scheme 2. Two main initial synthetic steps for the synthesis of azolium salts of N-tethered naphthalimide complexes. Bold numbers are those of the final complexes presented in Fig. 2 and 3 that have subsequently been synthesised using these precursors.

Azolium salt precursors of complexes **13a-h** were synthesised by reacting 4-chloro-N-alkyl-naphthalimide (Scheme 1) with N-ethyl/phenylethylenediamine, followed by heating at 100 °C for 3h under N_2 atmosphere in the presence of triethyl orthoformate (Scheme 3) [39].

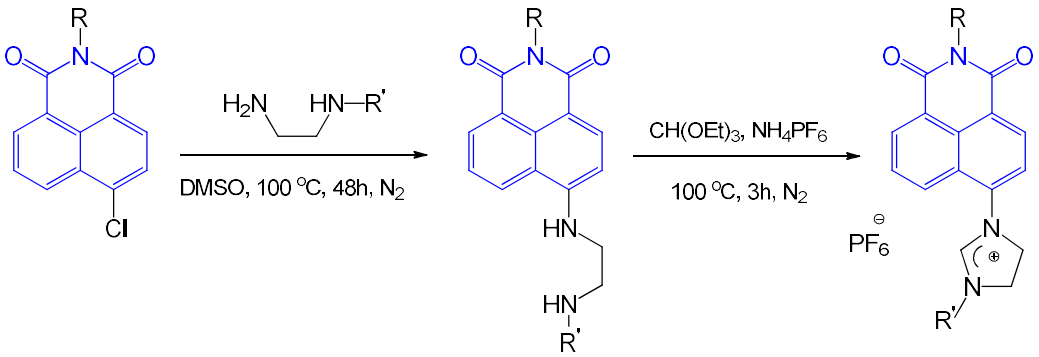

R = $(CH_2)_2O(CH_2)_2OH$ (**13a**, **13b**), $(CH_2)_2CH_3$ (**13c**, **13d**), Ph (**13e**, **13f**), $(CH_2)_7CH_3$ (**13g**, **13h**)
R' = Et (**13a**, **13c**, **13e**, **13g**), Ph (**13b**, **13d**, **13f**, **13h**)

Scheme 3. Synthesis of the azolium salts for complexes **13a-h**, starting from 4-chloro-N-alkyl-naphthalimide. Bold numbers are those of the complexes presented in Fig. 2 and 3 that have subsequently been synthesised using these precursors.

Since the complexes of scaffold **D** (**9-12**) contain two naphthalimide moieties, the quaternisation step in the synthesis of the azolium salts also involved reaction with a naphthalimide-containing alkyl halide, thus combining the two main synthesis strategies (Scheme 4). The naphthalimide-containing alkyl halide was synthesised by reacting 1,8-naphthalic anhydride with 25% ammonia and subsequently with 1,3-dibromopropane [38]. Reaction with one equivalent of the alkyl halide and refluxing in CH_3CN for three days afforded the products in 81% (R = H) and 58% (R = SCH_2CH_3) yield [38]. Interestingly, the complexes of scaffold **B** (**6a** and **6b**) are the only bimetallic complexes of this type reported in literature [32]. Complexes of scaffolds **B** and **D** (Fig. 2) as well as **N** (Fig. 3) are also the only NHC-complexes that contain two naphthalimide moieties [36,38].

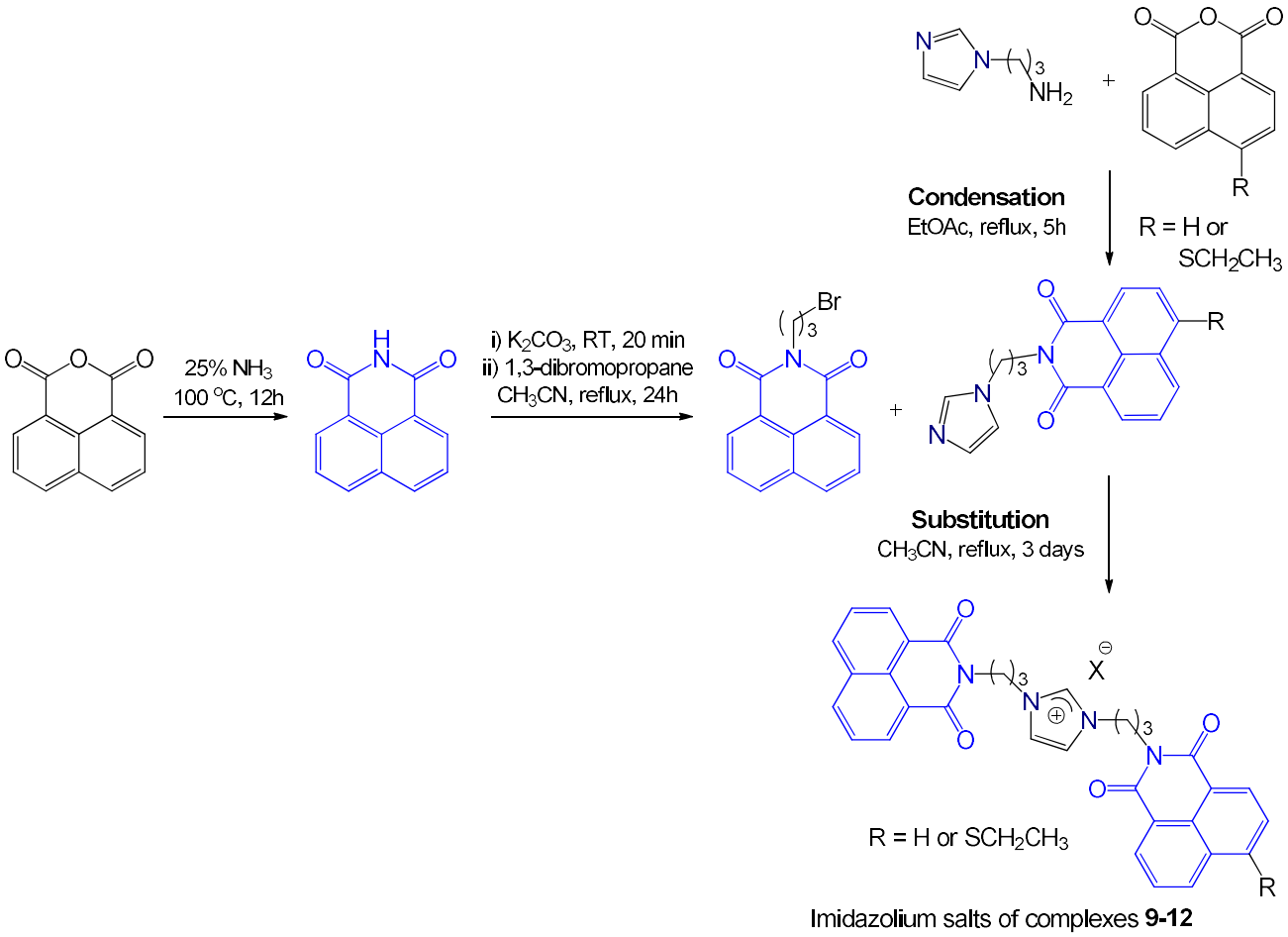

Scheme 4. Synthesis of the azolium salts for complexes **9-12** (scaffold **D**) by initial condensation and subsequent substitution.

Complexes **19** and **20**, presented by scaffold **G**, have a phenyl ethynyl linker between the imidazole ring and the naphthalimide moiety, demanding a different synthetic approach for the azolium salt (Scheme 5) than what has been described thus far for complexes tethered *via* a C-atom in the naphthalene rings. Having an unsaturated linker separating the naphthalimide and NHC moiety, denotes another structural variant represented by complexes of both scaffolds **C** and **G**. For complexes **19** and **20**, imidazole was reacted with *p*-bromofluorobenzene and K_3PO_4 in DMF at 150 °C, followed by two subsequent Sonogashira-Hagihara cross-coupling reactions, performed in toluene at 80 °C in the presence of both a copper and a palladium catalyst in combination with NEt_3 [41].

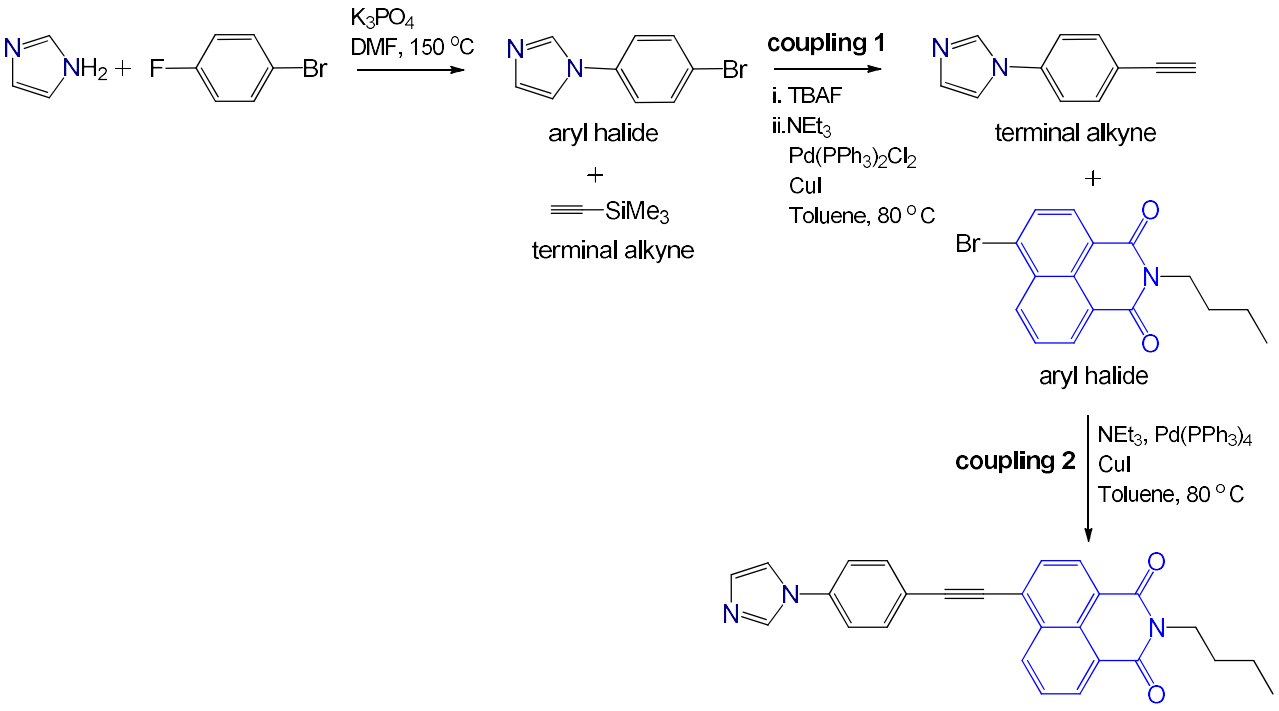

Scheme 5. Sonogashira-Hagihara cross-coupling reactions involved in the synthesis of the azolium salt for complexes **19** and **20**.

The first cross-coupling reaction (Scheme 5) allowed coupling of trimethylsilylacetylene to the imidazole aryl halide derivative, affording a terminal alkyne, after cleaving the Si-C bond with tetra-n-butylammonium fluoride (TBAF) [41]. The product of this reaction was then reacted with 4-bromo-N-(n-butyl)-1,8-naphthalimide in a second coupling reaction, affording the N-tethered imidazole-naphthalimide moiety in Scheme 5 [41]. The final quaternisation step was performed as described before, by refluxing in CH_3CN in the presence of excess MeI to afford the azolium salt in 63% yield [41].

Complexation to Rh(I) (**3**, **10**) [1,38,50], Ru(II) (**4**, **12**) [1,38,50], Ir(I) (**17b**) [44], Ir(III) (**21-23**) [45-47], Au(I) (**2**, **9** [38], **13** [39,41], **20** [41]) and Cu(I) (**14**, **19**) [41] was achieved by conventional methods, that involved an initial reaction with Ag_2O and subsequent transmetallation by refluxing overnight in DCM under an inert argon/N_2 atmosphere. For **13i-15** [41], **21** [45,46] and **22** [46], using 1,2-dichloroethane or dichlorobenzene as solvent instead, allowed the reaction to take place at higher temperatures (110-120 °C) while for **19** [41] and **20** [41] a mixture of DCM and CH_3NO_2 was used in addition to adding NaI during the initial step. For **17b** the reaction of the azolium salt with Ag_2O and subsequent transmetallation was performed in CH_3CN. Complexes **21d** and **23** were formed in reactions following a one-pot

method, whereby the azolium salt, Ag_2O, $[Cp^*Ir(\mu\text{-}Cl)Cl]_2$ and NBu_4I were refluxed overnight in CH_3CN to afford the regioisomers, **21d** and **23**, in a 1:1 ratio [47]. The respective (*R*)- and (*S*)-enantiomers of **21d** and **23** did not epimerise after being dissolved in CH_3CN for several days [47]. In the formation of the Rh(I) and Ir(I) complexes of **16a**,**b** and **17a**, direct metallation was achieved by the addition of DIPEA and refluxing the mixture overnight in dry DCM [44].

One of the metal-Cl bonds in **4b** exchanged for DMSO while for **3b** exchange could not be proven by ^1H NMR spectroscopy. Complex **5b** decomposed in a buffered solution with pH = 7.5, excluding it from studies regarding the anticancer mechanism [50]. Complexes **3e**, **3f** and **10b** precipitated out of a buffered solution with pH = 7.8 [1,38]. Complexes containing Rh(I), Ir(I) or Ru(II) were synthesised using common metal precursors $[RhCl(COD)]_2$ (**3**, **8**, **10**, **16**) [1,38,50], $[IrCl(COD)]_2$ (**17**) [44] or $[Ru(p\text{-cymene})Cl_2]_2$ (**4**, **12**) [1,38,50]. Au(I) complexes were synthesised using either $AuClS(CH_3)_2$ (**2** [42], **9** [38]) or C_4H_8AuClS (**13i** [41], **20** [41]) while for Cu(I) either $CuBr{\cdot}CH_3SCH_3$ (**5**) [50] or CuCl (**14**, **19**) [41] was used. Ir(III) complexes were formed using either $[Ir(C\text{^}N)_2Cl]_2$ (**21a-b**, **22**) [45,46] (where C^N refers to a cyclometallated phenylpyridine moiety, or a derivative thereof), or $[Cp^*Ir(\mu\text{-}Cl)Cl]_2$ (**21d**, **23**) [47] as reagents.

Complexation to Au(I) can also be achieved by adding the azolium salt and metal precursor directly in the presence of a base, similar to the syntheses of complexes **13a-h** [39]. The azolium salt, KO^tBu and C_4H_8AuClS were refluxed overnight in MeOH, under N_2 atmosphere with the exclusion of light [39]. Complexation with Ag(I) is achieved similarly when the azolium salt reacts directly with Ag_2O (**15**) [41] or AgOAc (**11**) [38] at room temperature in DCM with the exclusion of light. Instability of complex **15** [41] (Ag(I)) in DCM precluded it from subsequent photoluminescence studies.

Three slightly different methods were required for coordination to Pd(II), using either $PdCl_2$ (**1** [32], **6-8** [32,33], **24a** [34]) or $C_{46}H_{46}O_4P_2Pd_2$ (**24b**) [34] (trans-di(*m*-acetato)-bis[*o*-(di-*o*-tolylphosphino)benzyl]dipalladium(II) i.e. Herrmann′s catalyst) as metal reagent. Complexes **1** [32] and **6-8** [32,33] were synthesised when the azolium salt, $PdCl_2$, K_2CO_3, KBr and pyridine stirred at 80 °C for 16h. Complex **24a** [34] formed when $PdCl_2$ and N,N-dimethylbenzylamine were refluxed in CH_3CN and, after the solution turned dark orange, K_2CO_3 was added. This was followed by addition of the azolium salt when the solution became yellow and stirring was

continued at 50 °C for 18h. Complex **24b** [34] was synthesised by stirring the azolium salt, $C_{46}H_{46}O_4P_2Pd_2$ and K_2CO_3 in CH_3CN at 50 °C for 18h.

Post-modification of the heteroleptic bis-NHC Au(I) complex, **c** in Scheme 6, was necessary to yield **18**. Complex **c** was initially reacted with 4-nitrophenyl chloroformate to form precursor complex **d**. Complex **d** was subsequently reacted with the appropriate naphthalimide precursor to afford **18** in 40% yield. The coupling of compound **c** to various aliphatic and aromatic alcohols as well as amines to form respective carbonate- and carbamate-containing complexes have been studied by Sen *et al.* [40,52] for their biological applications. The synthesis of the naphthalimide precursor was previously shown in Scheme 1. Compounds **a** [53] and **b** [54] in Scheme 6 can be synthesised according to reported literature procedures. Complex **18** is the only cationic naphthalimide-NHC complex that has been reported in the literature to date.

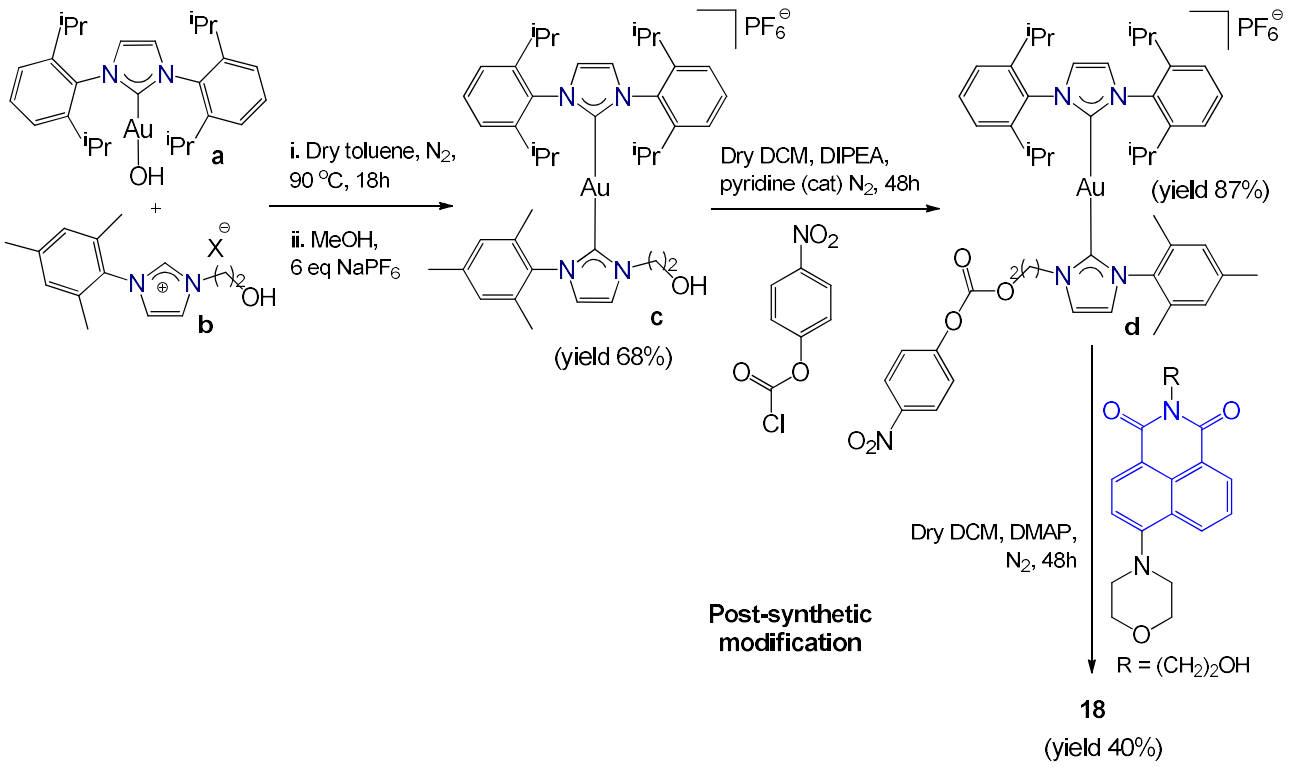

Scheme 6. Synthesis of complex **18**, involving post-modification of a heteroleptic bis-NHC complex **c** *via* intermediate **d**.

2.2 Complexes with a naphthalimide moiety connected to the NHC backbone

The synthesis of complexes with the naphthalimide moiety installed in the backbone of the NHC ligand can be challenging and examples in literature are limited. If the naphthalimide moiety is fused to the backbone as in complexes **26-29**, a ring-building method is required. For the NHC ligands of **26-29**, 3,4-diamino naphthalimide derivatives (Scheme 1) underwent ring-closure, as described for **13a-13h** in Scheme 3, by reacting with triethyl orthoformate in addition to methane sulfonic acid [14]. N-quaternisation occurred subsequently by reaction with excess 4-methylbenzyl chloride at 80 °C for 72h [34]. Synthesis of the azolium salt of **25** was achieved similar to most of the N-tethered complexes; with an initial condensation step (Scheme 2) involving 1,8-naphthalic anhydride and 4-(1H-benzimidazol-1-yl)aniline in DMF as solvent in the presence of K_2CO_3 [33]. The subsequent N-quaternisation step, however, afforded two inseparable isomers whereby the naphthalimide moiety is bonded to either one of the carbon atoms on the benzimidazolylidene ring. (Fig. 3) [33].

Complex **25** [33] was synthesised using the same method used for complexes **1** [32] and **6-8** [32,33] which involved the azolium salt, $PdCl_2$, K_2CO_3, KBr and pyridine stirring at 80 °C for 16h. Complex **26c** [35] was afforded when the azolium salt, *trans*-[$Pd(py_2(Cl)_2$] and K_2CO_3 were stirred in dry THF at 40 °C for 2h while **26a** [34] and **26b** [34] were yielded using the same respective methods as for **24a** [34] and **24b** [34]. For the formation of complexes **26d-h**, allyl-containing Pd(II) precursors, the respective azolium salt and K_2CO_3 were stirred in dry THF for 2h at room temperature [37]. The allyl-containing Pd(II) precursors were synthesised using reported literature methods [55-57]. Complexes **28** [36] and **29** [36] were synthesised when the azolium salt, metal precursor (dibromobis(1,3-diisopropylbenzimidazol-2-ylidene)dibromodipalladium (**28**) or *trans*-[$Pd(DMSO)_2(Cl)_2$] (**29**)) and K_2CO_3 were stirred in dry dioxane (**28**) or THF (**29**) at 40 °C for 18h. Complexes **28** and **29** together with **18** are the only biscarbene complexes with naphthalimide-NHC moieties that have been reported in the literature to date. Complexes **27a-e** [35,37] are also the only complexes containing a Pt(II) centre. Complex **27a** was formed in the reaction of the azolium salt with *cis*-[$Pt(DMSO)_2(Cl)_2$] and K_2CO_3, stirring in dry THF at 40 °C for 18h [35]. Post-modification of **27a** at 50 °C by reaction with either PPh_3 in chloroform for 4h, pyridine for 18h or 4-dimethylaminopyridine in chloroform for 18h afforded complexes **27b-d**, respectively [35]. Complex **27e** was synthesised using the same method as **26d-h** [37].

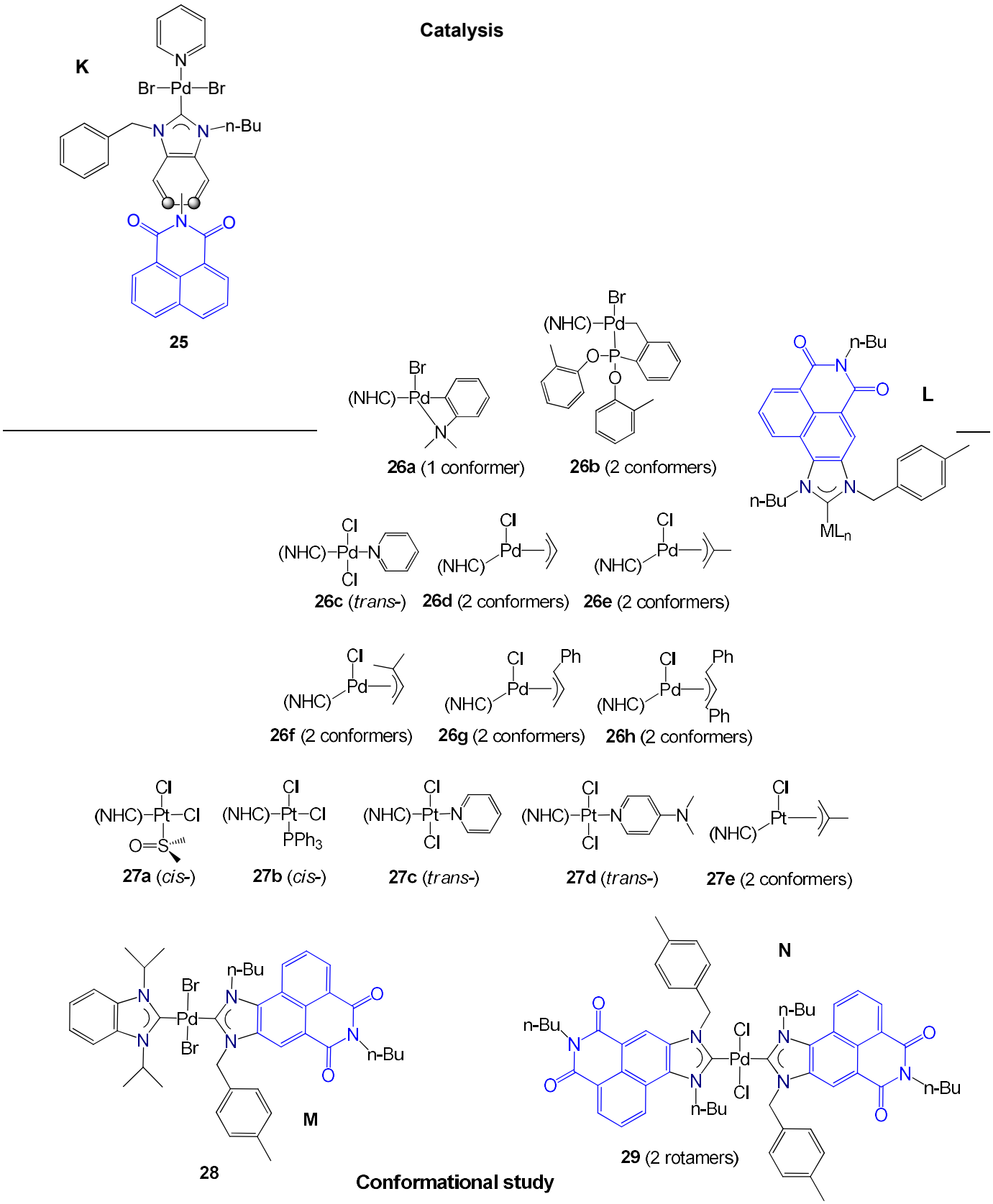

Fig. 3. Naphthalimide-NHC complexes with the naphthalimide moiety connected to the NHC backbone, classified according to their application and grouped into four basic scaffolds (**K-N**). Overlap between application fields is indicated by bridging structures.

Azolium salts and the corresponding complexes were all characterised with ^{1}H and ^{13}C NMR spectroscopy. Several complexes were synthesised in yields below 50%. These are highlighted in yellow in Table 1. Many authors also reported using 2D NMR techniques such as HSQC and NOESY in their characterisation of the complexes [34-37,46,47]. The ^{13}C NMR spectra of five sets of complexes (**13i** and **14** [41], **16a** and **17a** [44], **19** and **20** [41], **26c** and **27c** [35] as well as **26e** and **27e**) [37] point to an additional interesting aspect. Among these respective complex sets, the influence of the metal can be evaluated since they are in the same oxidation state and otherwise identical. $C_{carbene}$ ^{13}C NMR signals of the Pt(II) (**27c** (155.9 ppm) [35], **27e** (188.7 ppm) [37]), Ir(I) (**17a** (182.2 ppm) [44] and Cu(I) (**14** (164.2 ppm), **19** (164.0 ppm)) [41] complexes are shifted upfield compared to their respective Pd(II) (**26c** (166.9 ppm) [35], **26e** (195.7 ppm) [37]), Rh(I) (**16a** (184.9 ppm)) [44] and Au(I) (**13i** (171.6 ppm), **20** (173.9 ppm)) [41] analogues. The apparent upfield shift may be due to greater π-backdonation from the metal if one considers that Pt(II) and Ir(I) are more electron-rich than Pd(II) [37] and Rh(I) [44], respectively and Cu(I) smaller in size than Au(I), thus affording better overlap during π-backdonation [58,59].

For complexes **21d** and **23** their respective (*R*)- or (*S*)-enantiomers were separated with chiral column chromatography [47]. A comparison of the circular dichroism spectra for the respective isomers showed a clear mirror-image, confirming their stability and resistance to epimerise [47]. As part of detailed conformational studies of complexes **24** [34], **26a-c** [34,35], **26d-h** [34,37], **27a-d** [35] and **27e** [35,37], isomers and conformers were studied using techniques such as COSY, NOESY, ^{31}P EXSY, ^{31}P-^{1}H HMBC correlation methods and low or high temperature NMR experiments together with DFT. During high temperature NMR experiments, complex **26d** decomposed above 80 °C [37]. Complexes **16a** and **17a** each existed as two rotamers that were distinguished with low temperature ^{1}H NMR spectroscopy [44].

Correlation between experimental NMR data and theoretical DFT-calculated thermodynamic parameters showed that complexes **27a** and **27b** have *cis*-conformations while **26c**, **27c** and **27d** have *trans*-conformations [35]. Complexes **24a**, **24b**, **26a** and **26b** were shown to exist as two, four, one and two distinct conformers, respectively [34]. Complexes **26d-h** and **27e** were shown to each exist as two conformers due to hindered rotation around the M-$C_{carbene}$ bond with experimental rotation barriers (13.1-17.2 kcal/mol) supported by DFT.

Similarly, for complex **29** [36] experimental NMR data and theoretical DFT-calculated thermodynamic parameters confirmed the presence of a *syn*-rotamer (with the same N-appended groups on the same side) and an *anti*-rotamer (with the same N-appended groups on the opposite side, see Fig. 3). Additionally, the bond order, bond length and bond strength were studied based on theoretical natural bond order (NBO) calculations and by comparing the experimental ^{13}C NMR spectra of complexes **28** and **29** [36]. This was done in accordance with a study by Huynh *et al.* whereby the σ-donor properties of an NHC ligand were interpreted with regard to the chemical shift of the $C_{carbene}$ ^{13}C NMR signal of co-ligated 1,3-diisopropylbenzimidazolin-2-ylidene [60].

Table 1
% Yield values and physical description of complexes and their azolium salts.

Complex	Metal	Yield (%)		Complex colour and form	Ref
		Naphthalimide-containing azolium salt	Complex		
1a	Pd(II)	95	71	Orange solid	[32]
1b		97	62	Pale yellow solid	
1c		98	65	Yellow solid	
1d		97	60		
1e		95	58		
2a	Au(I)	90	33	White powder	[42]
2b		55	10		
2c		79	11		
2d		n.d.	n.d.		
3a	Rh(I)	n.d.	23	Yellow crystals	[50]
3b			53		
3c			76	Yellow solid	
3d			46	Dark yellow/brown solid	[1]
3e		98	63	Dark yellow solid	
3f		61	64	Light yellow solid	
4a	Ru(II)	n.d.	47	Red/brown solid	[50]
4b			58	Red/brown crystals	
4c				Red/brown solid	
4d			47	Red solid	[1]
4e		98	64		
4f		61	54	Dark yellow/brown solid	
5a	Cu(I)	n.d.	40	White solid	[50]
5b					
5c			87		
6a	Pd(II)	95	45	Yellow solid	[32]
6b		85	41		
7		94	71		[33]
8		93	53		
9a	Au(I)	81	47	White solid	[38]
9b		58	45	Dark yellow solid	

10a	Rh(I)	81	63		
10b		58	45		
11a	Ag(I)	81	44	White solid	
11b		58	63	Brown solid	
12a	Ru(II)	81	38	Dark red solid	
12b		58	66		
13a	Au(I)	54	81	Grey solid	[39]
13b		64	84	Grey-yellow solid	
13c		50	45	Off-white solid	
13d		81	85	Grey solid	
13e		67	n.d.	n.d.	
13f		85	49	Grey solid	
13g		74	68	Grey-yellow solid	
13h		54	79	Grey solid	
13i		80	72	Off-white solid	[41,45]
14	Cu(I)		30	Yellow solid	
15	Ag(I)		94	Green solid	
16a	Rh(I)	45	71	Bright red solid	[40,44]
16b		69	29	Yellow solid	
17a	Ir(I)	45	66	Bright red solid	
17b		69	22	Yellow solid	
18	Au(I)	NA	40	Yellow microcrystalline powder	[40]
19	Cu(I)	63	63	Yellow solid	[41]
20	Au(I)		33		
21a	Ir(III)	80	40	n.d.	[45,46]
21b			70		
21c			53		
21d			33	Crystalline red powder	[47]
22a		72	75	n.d.	[46]
22b			51		
22c			30		
23		80	39	Crystalline red powder	[47]
24a	Pd(II)	n.d.	92	White solid	[34]
24b			90		
25		91	61	Yellow solid	[33]
26a		90	80	Pale yellow solid	[14,34]
26b			83		
26c			63		[14,35]
26d			90	Yellow solid	[14,37]
26e			87		
26f			73		
26g			65		
26h			90	Amber solid	
27a	Pt(II)		88	Pale yellow solid	[14,35]
27b			61		
27c			95		
27d			59		
27e			90	Yellow solid	[14,37]
28	Pd(II)		95	Pale yellow solid	[14,36]
29			72		

n.d. = not determined
NA = not applicable; **18** was not synthesised using a naphthalimide-containing azolium salt
Complexes highlighted in yellow were obtained at yields below 50%.

Most authors reported MS and elemental analysis data for the complexes while some included melting point and IR data as well. Table 2 provides an account of the complexes for which single crystals were obtained and highlights some of the data. For **21d** and **23** crystals of the racemic mixtures that contain both (*R*)- and (*S*)-enantiomers, with non-covalent interactions between the N-butyl group and the naphthalimide moiety of the other isomer, were isolated [47]. Fig. 4 and 5 illustrate the SCXRD (single crystal X-ray diffraction) structure obtained for **13c**, showing that the imidazolinylidene and naphthalimide ring planes are not parallel with respect to one another even though π-π stacking is observed. Crystals for the azolium salts of complexes **13c** [39] **16a**,**b** [44] and **21** [46] were also obtained.

Table 2
Highlighted SCXRD data.

Complex	$C_{carbene}$-M bond length (Å)	M–M interactions (Å)	π–π stacking	Ref
1a (Pd(II))	1.960(5)	No	No	[32]
1c (Pd(II))	1.959(2)	No	No	
4b (Ru(II))	2.090(2)	No	No	[50]
7a (Pd(II))	1.950(5)	No	No	[33]
13c (Au(I))	1.984(2)	Yes (3.314(6))	Yes	[39]
13i (Au(I))	1.985(5)	Yes (3.407(1))	Yes	[41]
16a (Rh(I))	2.027(3)	No	Yes	[44]
16b (Rh(I))	2.035(4)	No	Yes	
18 (Au(I))	2.12(4)	No	Yes	[40]
21a (Ir(III))	2.077(1)	No	Yes	[45,46]
21b (Ir(III))	2.063(3)	No	Yes	[46]
21c (Ir(III))	2.069(3)	No	Yes	
22c (Ir(III))	2.052(3)	No	Yes	[46]
***(R)*-23** (Ir(III))	2.03(2)	No	Yes	[47]

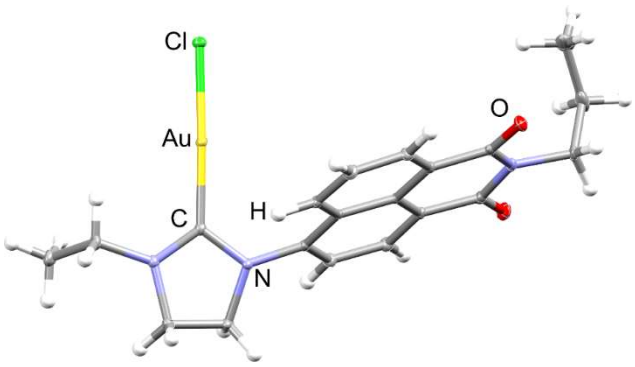

Fig. 4. SCXRD structure of **13c**. Thermal ellipsoids have been drawn at 50%. Colour scheme: Au (yellow), chloride (green), carbon (grey), hydrogen (white), oxygen (red), nitrogen (blue-violet).

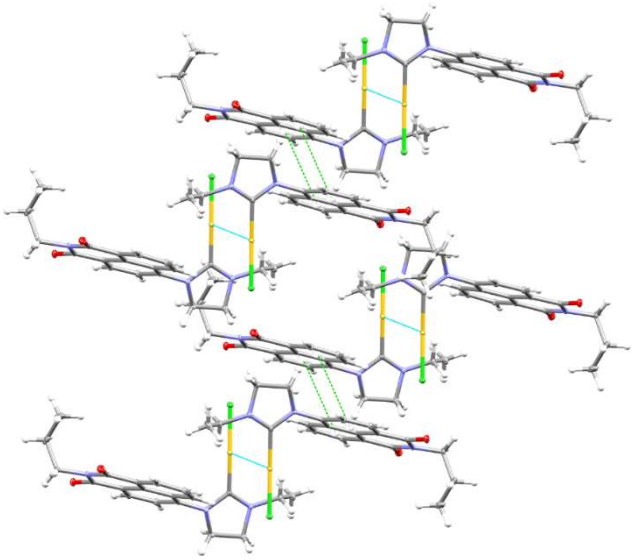

Fig. 5. Packing of **13c** showing π-π stacking interactions (green dashed lines) and aurophilic interactions (teal lines). Colour scheme: Au (yellow), chloride (green), carbon (grey), hydrogen (white), oxygen (red), nitrogen (blue-violet).

3. Applications

3.1 Catalysis

3.1.1 Larock heteroannulation reaction

Panyam *et al.* [32,33] investigated the efficiency of complexes **1a-e**, **6**, **7**, **8** and **25** in Larock heteroannulation when reacting *o*-haloanilines and disubstituted alkyne derivatives in a 1:2 ratio (Scheme 7). A limited number of metal NHC complexes have been studied in catalysing Larock-type heteroannulation reactions. Scheme 7 depicts four sets of optimal reaction conditions (**a-d**) that led to the regioselective formation of heteroannulated products. Complex **1c** showed the highest activity (TOF between 0.9 h^{-1} for reaction **b** (Table 4, entries 26 and 31) and 2.3 h^{-1} for reaction **d** (Table 4, entry 41)) among **1a-e**, **6**, **7**, **8** and **25**. All of the complexes did, however, perform better than the conventional catalysts $Pd(OAc)_2$ and PPh_3 (TOF of 0.6 h^{-1} for reaction **b**) or 1,10-phenantroline and $Pd(OAc)_2$ (TOF of 0.5 h^{-1} for reaction **b**) [32,33]. The catalytic activities of complexes **7** and **8**, having constrained naphthalimide moieties, also compared well with **1c** when tested for reactions **c** and **d** (Scheme 7) [33].

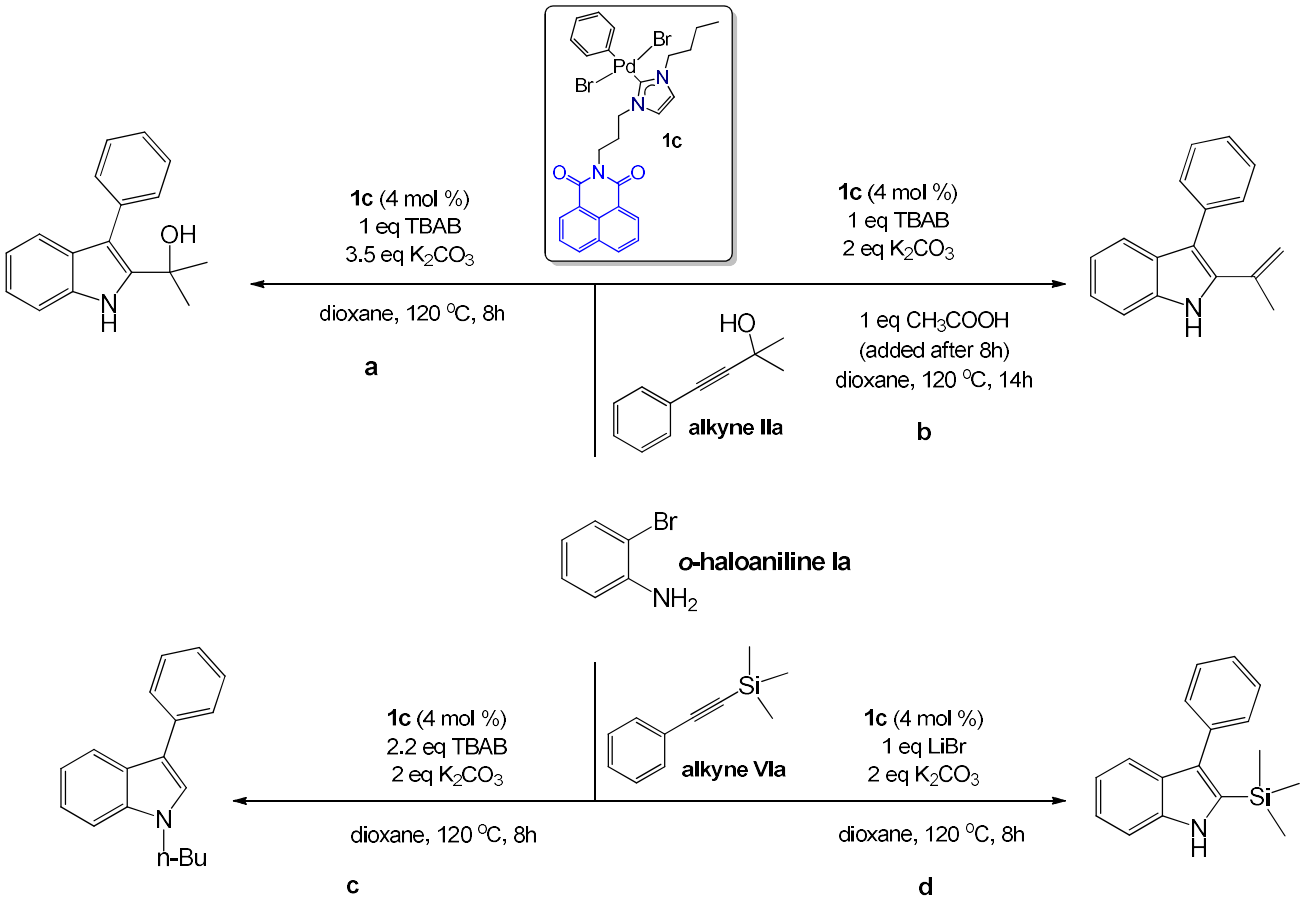

Scheme 7. Optimised reaction conditions for catalytic selective Larock heteroannulation.

In general, conditions were optimised using substrates **Ia**, **IIa** and **VIa** (Table 3), by varying the catalyst loading and reaction temperature in addition to screening different acids, bases, solvents and additives [32,33]. It was found that the specific additive added to the reaction as well as the relative amounts of base and additives were critical to the exclusive formation of target compounds [32,33]. For reaction **a**, during optimisation of reaction conditions, increasing the relative amount of K_2CO_3 added from 2 to 3.5 equivalents afforded the hydroxy product selectively. When considering reaction **b**, addition of 2 equivalents of K_2CO_3 and a subsequent addition of CH_3COOH selectively produced the dehydrated product, while addition of 2 equivalents of K_2CO_3 and no CH_3COOH resulted in a mixture of the hydroxy and dehydrated products [32]. For reaction **c**, increasing the relative amount of TBAB added, from 1 to 2.2 equivalents, afforded N-butyl-3-aryl-indole selectively while 1 equivalent yielded a mixture that also contained 3-aryl-1H-indole. For reaction **d**, 1 equivalent of LiBr, instead of TBAB, afforded 3-aryl-2-(trimethylsilyl)-1H-indole selectively [33].

Table 3
Substrate scope for the Larock heteroannulation reaction.

***o*-Haloaniline**			
Substrate	**X**	**R^1**	**R^2**
Ia	Br	H	H
Ib	Cl	H	H
Ic	I	H	H
Id	F	H	H
Ie	Br	$COCH_3$	H
If	Br	$COCF_3$	H
Ig	Br	Me	H
Ih	Br	*n*-C_4H_9	H
Ii	Br	H	Me
Ij	Br	H	OMe
Ik	Br	H	F
Il	Br	H	CN
Im	Br	H	EtOOC
In	Br	H	MeCO
Alkyne			
Substrate	**R^3/R^6**	**R^4**	**R^5**
IIa, IIIa, VIa	H	Me	Me
IIb	H	Et	Et
IIc	H	Me	Et
IId	H	Ph	Me
IIe	H	Ph	Et
IIf	H	4-MeC_6H_4	Me
IIg	H	4-$MeOC_6H_4$	Me
IIh	H	biphenyl	Me
IIi, IIIb, VIb	Me	Me	Me
IIj, IIIc, VIc	OMe	Me	Me
IIk, VId	Fused benzene	Me	Me
III, IIId, VIe	CN	Me	Me
IIm, IIIe, VIf	NO_2	Me	Me
IIn	MeCO	Me	Me

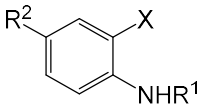

I

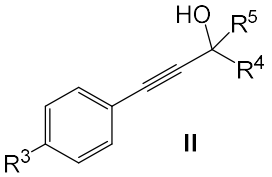

II

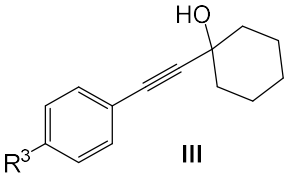

III

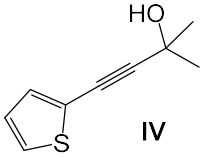

IV

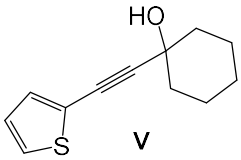

V

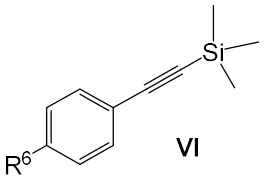

VI

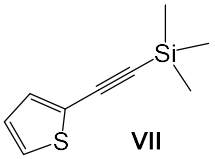

VII

For reaction **c** TBAB, TBAF, tetraethylammonium bromide, tetrapropylammonium bromide, methyltrioctyl ammonium chloride or tetramethylammonium chloride could be used as

additive [33]. TBAB was however preferred while reaction **d** required LiBr instead [33]. Elementary mechanistic steps were envisioned to be coordination of the alkyl halide by oxidative insertion, followed by insertion of the alkyne in the Pd-C bond, directed by the OH-group (for reactions **a** and **b**), followed by the release of HBr [32,33]. After HBr evolution the product that formed depended on the presence (or absence, for reaction **a**) of specific additives (CH_3COOH (reaction **b**), TBAB (reaction **c**) or LiBr (reaction **d**)) [32,33].

The study aimed to prove the effectiveness and applicability of the method(s) by investigating a large scope of substrates (Table 3), scaling up and derivatising products into consequent synthetically useful synthons, in addition to postulating reaction mechanisms [32,33]. The possible directing effect of the naphthalimide moiety on the catalytic activity through π-π stacking interactions using aromatic additives was evaluated. Addition of aromatic additives (anthracene, pyrene and naphthalimide), capable of also interacting with the naphthalimide moiety, decreased the catalytic activity [32]. The substrate scope considered different halogens, N-functionalities, incorporating electron-donating or -withdrawing groups at the *para*-positions as well as chiral or achiral tertiary propargylic alcohols [32,33]. Table 3 and Table 4 provide summaries of the studied substrates and reactions, totalling 50 unique substrate pairings and 62 reactions represented by **b**, **c** and **d** (Scheme 7).

Table 4
Isolated yields (%) for the studied Larock heteroannulation reactions.

Entry	*o*-Haloaniline	alkyne	Isolated yield (%)			Ref
			b	c	d	
1	**Ia**	**IIa**	77	n.d.	n.d.	[32]
2	**Ib**		70	n.d.	n.d.	
3	**Ic**		81	n.d.	n.d.	
4	**Id**		11[a]	n.d.	n.d.	
5	**Ie**		70	n.d.	n.d.	
6	**If**		71	n.d.	n.d.	
7	**Ig**		71	n.d.	n.d.	
8	**Ih**		70	n.d.	n.d.	
9	**Ii**		75	n.d.	n.d.	
10	**Il**		68	n.d.	n.d.	
11	**Im**		66	n.d.	n.d.	
12	**In**		63	n.d.	n.d.	

13	**Ij**		72	n.d.	n.d.	
14	**Ik**		69	n.d.	n.d.	
15		**IIb**[b]	71	n.d.	n.d.	
16		**IIc**	61[d]	n.d.	n.d.	
17		**IId**	65	n.d.	n.d.	
18		**IIe**	63[d]	n.d.	n.d.	
19		**IIf**	62	n.d.	n.d.	
20		**IIg**	60	n.d.	n.d.	
21		**IIh**	58	n.d.	n.d.	
22		**IIi**	76	n.d.	n.d.	
23		**IIj**	72	n.d.	n.d.	
24	**Ia**	**IIk**	62	n.d.	n.d.	
25		**III**	61	n.d.	n.d.	
26		**IIm**	52	n.d.	n.d.	
27		**IIIa**	69	n.d.	n.d.	
28		**IIIb**	65	n.d.	n.d.	
29		**IIIc**	63	n.d.	n.d.	
30		**IIId**	57	n.d.	n.d.	
31		**IIIe**	52[c]	n.d.	n.d.	
32		**IV**	53	n.d.	n.d.	
33		**V**	54	n.d.	n.d.	
34		**III**	60	n.d.	n.d.	
35	**Ii**	**IIm**	54	n.d.	n.d.	
36		**IIIa**	65	n.d.	n.d.	
37		**IV**	57	n.d.	n.d.	
38	**Ia**		n.d.	65,[f] 67,[g] 60,[h] 51,[i] 23,[j] 42[k]	71, 69[e]	
39	**Ib**		n.d.	n.d.	63	
40	**Ic**		n.d.	n.d.	82	
41	**Ii**	**VIa**	n.d.	67	73	
42	**Il**		n.d.	58	61	
43	**Im**		n.d.	57	60	[33]
44	**In**		n.d.	60	65	
45		**VIb**	n.d.	n.d.	71	
46		**VIc**	n.d.	n.d.	69	
47	**Ia**	**VId**	n.d.	55	68	
48		**VIe**	n.d.	n.d.	63	
49		**VIf**	n.d.	n.d.	59	
50		**VII**	n.d.	n.d.	62	

General reaction conditions **b**: *o*-Haloaniline (1 mmol), alkyne (2 mmol), 1c (4 mol%), K_2CO_3 (2 eq), TBAB (1 eq), 120 °C, 8 h, dioxane (2 mL), CH_3COOH (1 eq) 6h
General reaction conditions **c**: *o*-Haloaniline (1 mmol), alkyne (2 mmol), 1c (4 mol%), K_2CO_3 (2 eq), TBAB (2.2 eq), dioxane (2 mL), 120 °C, 12 h.
General reaction conditions **d**: *o*-Haloaniline (1 mmol), alkyne (2 mmol), 1c (4 mol%), K_2CO_3 (2 eq), LiBr (1 eq), dioxane (2 mL), 120 °C, 8 h.
[a]160 °C 48h; [b]24h; [c]Isomers *E/Z* (4:5); [d]Isomers *E/Z* (3:2); [e]Gram-scale; [f]Tetrabutylammonium fluoride; [g]Tetraethylammonium bromide; [h]Tetrapropylammonium bromide; [i]Methyltrioctyl ammonium chloride; [j]Tetramethylammonium chloride.
n.d. = not determined

Through their efforts, Panyam *et al.* [32,33] were thus able to synthesise compounds with 3-arylindole, 2-alkylindole and heteroarylsilane scaffolds that are pertinent in pharmaceutical, agrochemical and other fields. They have provided an effective one-pot method, that avoided using harsh oxidants, did not produce by-products and relied on air and moisture stable catalysts [32,33].

3.1.2 Suzuki-Miyaura reaction

Dangalov *et al.* [34] studied the application of **26a**,**b** in Suzuki-Miyaura coupling reactions between 4-bromoanisole and phenylboronic acid, reacted in a 1:1.5 ratio (Scheme 8).

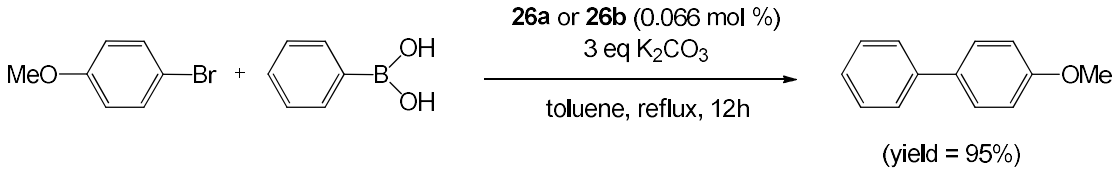

Scheme 8. Optimised reaction conditions for Suzuki-Miyaura reaction.

Conditions were optimised by screening of different solvents, reaction temperatures and bases in addition to performing reactions at various catalyst loadings (0.1 mol %, 0.033 mol % and 0.066 mol %) under an argon atmosphere or in air [34]. Solvents that were considered included water, DME, DME:H_2O (5:1), dioxane, dioxane:H_2O (5:1), CH_3CN, CH_3CN:H_2O (5:1), isopropyl alcohol, ethanol and toluene while the bases screened were K_2CO_3, Cs_2CO_3, CsF, K_3PO_4 and $Ba(OH)_2$ [34]. Conditions were finally optimised for toluene (Scheme 8), as it is less toxic, even if the reaction in DME:H_2O (5:1) with K_3PO_4 and a lower catalyst loading of 0.033 mol % of **26a** gave an appreciable yield of 85% [34].

3.2 Biological application

The biological application of metal NHC complexes is becoming increasingly more popular [61]. Many metal NHCs show anticancer, antibacterial and fungicidal properties in addition to often allowing for cellular imaging due to luminescent properties [61]. In terms of cancer research, various biomolecules can be targeted, depending on the metal as well as the particular NHC ligand scaffold and the type of cancer [61]. For bacteria and fungi, the biomolecular targets and the mechanism by which NHC complexes act on the targets, have received little attention. Only a few recent reports mention the slow release of metal ions inside bacterial cells from organometallic complexes as a key step in the mode of action [62]. It is suggested that the NHC complexes may target the cell's morphological structure [61].

The enzyme thioredoxin reductase (TrxR), which is responsible for maintaining the redox balance in cells, and DNA are the two most common biomolecular targets in cancer cells but the mechanism by which organometallic drugs act on these biomolecules are often not fully understood [63]. NHC complexes containing ruthenium-arene moieties have been illustrated to show an affinity for selenocysteine, present in TrxR [63]. Auranofin (Fig. 6) is an Au(I)-phosphine complex and well-known TrxR inhibitor that has been successfully applied as a therapeutic agent against rheumatoid arthritis [64]. It has recently been considered as an anticancer agent for its potential activity against aggressive breast, ovarian and lung cancer cells [64]. Naphthalimide-containing analogues (Fig. 6) of auranofin have shown appreciable anticancer activity against breast (MCF-7) and colorectal (HT-29) cancer cells with respective IC_{50} values ranging between 1.1–3.7 and 2.0–3.2 μM [65].

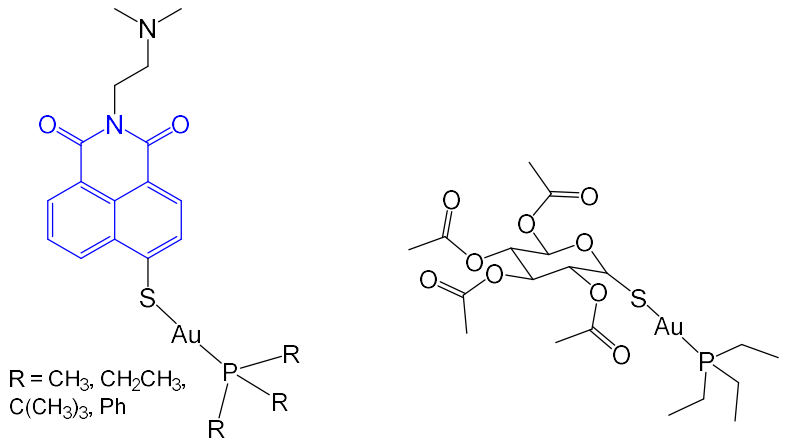

Auranofin-naphthalimide analogues[65] Auranofin[64]

Fig. 6. The TrxR inhibitor auranofin and naphthalimide-containing analogues.

In addition to conventional, right-handed B-DNA as originally described by Watson and Crick various secondary DNA structures that may be targeted are G-tetrad, left-handed Z-DNA, bent DNA, sticky DNA, cruciform and triplexes, among other [66]. Additional enzymes that can also be targeted in cancerous cells include glutathione reductase (GR), deubiquitinase (DUB), cyclooxygenase (COX) and cathepsin B [67]. Principally, organometallic complexes can bind to DNA by direct, irreversible coordination of the metal, which is influenced by the presence of ligands such as Cl^- that are easily hydrolysed as well as NHC ligand bulkiness [67]. NHC ligand structures are often altered for the sake of lipophilicity, chirality, multinuclearity and photo-activation in order to influence interactions with the biomolecular targets [63]. It is also common to combine metal fragments with biologically relevant compounds, for example naphthalimide, chloroquine, caffeine and many more [63,67]. Ultimately, modifications to NHC ligand scaffolds often result in these complexes having dual functionality whereby interaction with DNA occurs through coordination as well as non-covalently by intercalation or stacking [67].

When interactions with DNA inhibit the Topo II enzyme, thus interfering with the DNA's topology, cytotoxicity is effected as transcription is prevented [24]. DNA aggregation is a common consequence [67]. Furthermore, metal NHC complexes that contain Au(I) and Cu(I) have been shown to act oxidatively to damage DNA by reducing molecular oxygen to a reactive superoxide species [61,63,67]. Cell death mechanisms are typically intricate and finely interrelated; when complexes accumulate in mitochondria they can cause the release of the pro-apoptotic protein cytochrome c, which activates endonucleases and causes cell death by cleaving DNA [68].

Since the antiproliferative properties of 1,8-naphthalimides were first discovered by Brana and colleagues in 1973 [23], many structural variants have been synthesised to improve sensitivity and selectivity, invoke different modes of action or effect multiple mechanisms of interaction with DNA. An account by Tandon *et al.* summarised the possible structural variations that may increase cytotoxicity as 'imide substitution', 'ring-substitution', 'bis-naphthalimide', 'heterocyclic hybrid' and 'metal complexes' all of which are well represented herein [24]. Complexes of scaffolds **A**, **B**, **D-F** and **H-J** are heterocyclic hybrids with **6** [32], **9-12** [38] and **29** [36] having bis-naphthalimide moieties and **2d** [42], **3-4d-f** [1,43] and **9b-12b** [38] having an ethylthio-substituent at the *para*-position.

In a study by Kilpin *et al.* [69] it was shown that a series of naphthalimide-tagged Ru(II) complexes (Fig. 7), closely related to the complexes reviewed herein, had appreciable anticancer activity against ovarian carcinoma (A2780 and A2780R) cells. During preliminary mechanistic studies, the complexes were shown to intercalate into DNA *via* the naphthalimide moiety while the Ru(II) centre preferentially bonded to proteins, thus targeting two different biomolecules [69].

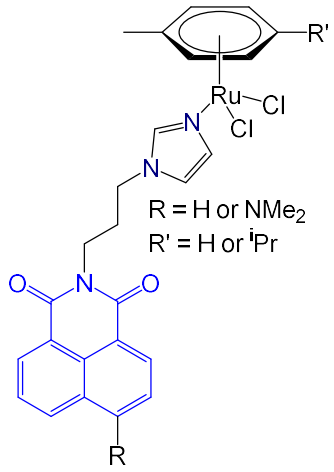

Naphthalimide-tagged Ru(II) complex[69]

Fig. 7. Naphthalimide-tagged Ru(II) complexes bonded *via* an imidazole N-atom, acting against cancerous cells through a dual mechanism.

3.2.1 Anticancer activity

Table 5
The IC_{50} values of complexes acting against cancerous cells, as a measure of potency.

Complex	Metal	IC_{50} (μM)[a]						Ref
		HT-29	MCF-7	LOVO	A549	PC3	TrxR	
cisplatin	Pt(II)	7.0 ± 2.0	2.0 ± 0.3	n.d.	n.d.	n.d.	n.d.	[70]
auranofin		n.d.	n.d.	n.d.	2.23 ± 0.12	n.d.	n.d.	[40]
2a		4.0 ± 0.7	4.6 ± 1.5	n.d.	n.d.	n.d.	0.28 ± 0.12	
2b	Au(I)	4.9 ± 1.8	6.3 ± 0.6	n.d.	n.d.	n.d.	n.d.	[42]
2c		18.2 ± 5.9	5.8 ± 2.9	n.d.	n.d.	n.d.	n.d.	
2d		1.9 ± 0.3	2.1 ± 0.5	n.d.	n.d.	n.d.	0.40 ± 0.13	
3a		5.1 ± 0.9	3.7 ± 0.1	n.d.	n.d.	n.d.	n.d.	
3b		4.6 ± 0.3	3.7 ± 0.1	n.d.	n.d.	n.d.	n.d.	[50]
3c	Rh(I)	9.8 ± 0.2	4.0 ± 0.2	n.d.	n.d.	n.d.	n.d.	
3d		10. 0 ± 0.4	5.8 ± 0.5	n.d.	n.d.	n.d.	n.d.	[1,43]
3e		6.5 ± 0.4	1.7 ± 0.3	n.d.	n.d.	n.d.	n.d.	

3f		6.2 ± 0.4	4.0 ± 0.4	n.d.	n.d.	n.d.	n.d.	
4a	Ru(II)	>100	55.4 ± 1.3	n.d.	n.d.	n.d.	n.d.	[50]
4b		>100	>100	n.d.	n.d.	n.d.	n.d.	
4c		14.2 ± 1.1	6.4 ± 0.6	n.d.	n.d.	n.d.	n.d.	
4d		36.8 ± 1.3	18.6 ± 1.3	n.d.	n.d.	n.d.	n.d.	[1,43]
4e		26.4 ± 1.1	11.6 ± 1.0	n.d.	n.d.	n.d.	n.d.	
4f		4.9 ± 0.02	4.8 ± 0.1	n.d.	n.d.	n.d.	n.d.	
5a	Cu(I)	>100	27.4 ± 2.1	n.d.	n.d.	n.d.	n.d.	[50]
5b		45.4 ± 3.6	14.8 ± 0.8	n.d.	n.d.	n.d.	n.d.	
5c		3.1 ± 0.8	2.0 ± 0.2	n.d.	n.d.	n.d.	n.d.	
9a	Au(I)	13.7 ± 1.2	7.4 ± 0.2	n.d.	n.d.	n.d.	n.d.	[38]
9b		11.3 ± 1.3	5.6 ± 1.0	n.d.	n.d.	n.d.	n.d.	
10a	Rh(I)	>100 (75%)	14.7 ± 1.6	n.d.	n.d.	n.d.	n.d.	
10b		2.7 ± 0.1	2.6 ± 0.03	n.d.	n.d.	n.d.	n.d.	
11a	Ag(I)	0.6 ± 0.03	0.2 ± 0.02	n.d.	n.d.	n.d.	n.d.	
11b		0.6 ± 0.03	0.5 ± 0.03	n.d.	n.d.	n.d.	n.d.	
12a	Ru(II)	>100 (66%)	26.0 ± 1.1	n.d.	n.d.	n.d.	n.d.	
12b		3.7 ± 0.1	1.7 ± 0.2	n.d.	n.d.	n.d.	n.d.	
13a	Au(I)	n.d.	84.21 ± 11.38	68.94 ± 2.29	>100	>100	n.d.	[39]
13b		n.d.	62.88 ± 5.58	91.64 ± 3.20	>100	>100	n.d.	
13c		n.d.	48.58 ± 10.58	>100	>100	>100	n.d.	
13d		n.d.	27.79 ± 11.89	41.54 ± 2.88	>100	>100	n.d.	
13f		n.d.	46.21 ± 13.01	49.10 ± 7.97	>100	>100	n.d.	
13g		n.d.	41.75 ± 9.34	50.92 ± 6.20	>100	46.63 ± 0.71	n.d.	
13h		n.d.	4.82 ± 0.77	40.99 ± 11.08	>100	>100	n.d.	
18		n.d.	n.d.	n.d.	0.072 ± 0.004	n.d.	n.d.	[40]
18-BSA[b]		n.d.	n.d.	n.d.	0.059 ± 0.003	n.d.	n.d.	

[a] Values are given as the mean of independent sets of data ± the standard error of the mean (SEM) for **2-5**, **9-12**, **18**, **18**-BSA as well as cisplatin and auranofin or the standard deviation (SD) for **13**.
[b] Complex **18** bonded to bovine serum albumin (BSA)
n.d. = not determined

Table 5 provides the IC_{50} values (half maximal inhibitory concentration [71]) reported for complexes **2-5** [1,42,43,50], **9-13** [38,39] and **18** [40] acting on cancerous breast (MCF-7), prostate (PC3), colorectal (HT-29 and LOVO) and lung (A549) cell lines, as well as the thioredoxin reductase (TrxR) protein. Complexes **2a** and **2d** [42] were selective towards TrxR with reference to untargeted glutathione reductase while complexes **3f** and **4f** [43] were mildly toxic against non-tumorigenic human foreskin fibroblasts. Data on the selectivity of the other complexes were not reported. Most complexes were more cytotoxic (lower IC_{50} values) than

the free azolium salts, warranting the exclusion of the reported IC_{50} values for the precursors herein. The free azolium salts of **13a-h** were shown to be more cytotoxic than their respective complexes [39]. Compared to cisplatin, which had IC_{50} values of 7.0 ± 2.0 μM (HT-29) and 2.0 ± 0.3 μM (MCF-7), 44% and 12% of the complexes in Table 5 performed better, respectively [70]. IC_{50} values for LOVO, A549 and PC3 cells are mostly significantly higher than for HT-29, MCF-7 and TrxR. Complex **18** and the **18**-BSA adduct however had remarkably low IC_{50} values against A549 cells and were more cytotoxic than auranofin. Bonding of **18** to bovine serum albumin (BSA), a blood protein, was shown to increase **18**'s stability by preventing hydrolysation [40,72]. The **18**-BSA adduct showed increased solubility under mimicked physiological conditions, which would facilitate its uptake and had comparable cytotoxicity to that of **18** on its own [40].

Complexes **2d** [42], **5c** [50], **10b** [38], **11a** [38] and **11b** [38] had the strongest antiproliferative effects against HT-29 while MCF-7 cells were most sensitive towards complexes **3e** [1], **5c** [50], **11a** [38], **11b** [38] and **12b** [38]. Overall, the bis-naphthalimide Ag(I)-complexes **11a** [38] and **11b** [38] showed the highest activity against both HT-29 and MCF-7 cells, although Streciwilk *et al.* reported on the possible decomposition of these silver complexes and the possibility of their activity being due to the free azolium salts [38]. Except for complex **3** [1,43,50], an ethylthio-substituent at the *para*-position of the naphthalene rings in complexes of scaffold **A** and **D** improved the anticancer activity in both cell lines.

It is apparent that the cytotoxicity was higher with less sterically hindered methyl N-tethers for Au(I) complexes **2a-d** [42] while the more lipophilic benzyl tethers made Ru(II) complexes **4a-f** [1,42,43,50] more cytotoxic. For Au(I) complexes **13a-h**, replacing the N-ethyl substituent with a phenyl ring, thereby increasing lipophilicity, again increased cytotoxicity [39]. Additionally, the Rh(I) complexes **3a-f** were significantly more cytotoxic than their corresponding Ru(II) analogues **4a-f** [1,50]. Whether a complex is cationic or neutral might also play an important role which could account for the high cytotoxicity of complex **18** against A549 cells.

Au(I)-complexes **2a** and **2d** also showed activity against TrxR which compared well with values of previously studied cytotoxic Au(I)-phosphine complexes, ranging between 4.2–5.2 μM for HT-29 and 2.6–3.9 μM for MCF-7 cells [42,73]. The complexes were shown to be

selective towards TrxR, not inhibiting glutathione reductase at similar concentrations and were significantly more active than the free azolium salts [42].

Complex **3b** was also shown to be effective against Nalm-6 and resistant Nalm-6/VCR and Nalm-6/DNR leukaemia cells [50]. During mechanistic studies (*vide infra*), complexes **3f** and **4f** were tested against breast MDA-MB-231, colorectal HCT116 and p53-null HCT116 cells, with HCT116 being the most sensitive to **4f** within the first 24h [43].

3.2.2 Antimicrobial applications

The complexes successfully inhibited gram-positive bacterial strains (low MIC values) but were unsuccessful against *C. albicans* and gram-negative bacteria (Table 6). The Rh(I) complex **3f** showed the greatest overall inhibition, having an MIC value of 4 μg/mL against *S. aureus* (ATCC 43300) [1].

Table 6
Minimum inhibitory concentration (MIC) (μg/mL) of complexes against bacteria or fungi, as a measure of potency [1,38].

	Bacterial or Fungicidal strain	**MIC (μg/mL)**					
		3e (Rh(I))	**3f** (Rh(I))	**4e** (Ru(II))	**4f** (Ru(II))	**11a** (Ag(I))	**12a** (Ru(II))
Gram positive bacteria	*B. subtilis 168* (DSM 402)	16	16	16	8	16	16
	S. aureus (DSM 20231)	8	8	16	8	128	16
	S. aureus (ATCC 43300)	8	4	16	8	64	8
Gram negative bacteria	*E. coli* (DSM 30083)	>512	>512	>512	>512	256	>512
	A. baumannii (DSM 30007)	256	>512	256	>512	128	>512
	P. aeruginosa (DSM 50071)	>512	>512	256	>512	32	>512
Fungi	*C. albicans* (DSM 1386)	128	128	>512	>512	256	>512

In general, the Ru(II) complex **4f** had the best performance against all three gram positive bacterial strains [1]. The MIC values of $AgNO_3$ and commercial Ciprofloxacin against *S. aureus* and *E. coli* are 50 and 6.25 μL respectively, which clearly illustrates how well the complexes act against gram positive bacteria and how poorly against gram negative bacteria [74]. The inability of the complexes to inhibit *C. albicans* fungi is apparent when one considers the MIC value of 0.125 μg/mL for the commercial antifungal Fluconazole [75]. The complexes' ability to inhibit gram positive bacteria was also comparable to triazole-naphthalimide compounds that have been reported in the literature [11,12]. The compound shown in Fig. 1 (example 4) had MIC values (recorded at pH = 7.0) of 16, 1 and 2 μg/mL against *S. aureus*, *E. coli* and *C. albicans*, respectively [11].

3.2.3 Mechanistic studies

Double-stranded or G-quadruplex DNA conformations were studied as biomolecular targets. Streciwilk *et al.* performed a fluorescence resonance energy transfer (FRET) melting assay that screened interaction of **3e**, **3f** and **4f** against six different oligodeoxyribonucleotides, one with a double-stranded conformation and five with G-quadruplex conformations [1]. Interaction with DNA was investigated using atomic absorption spectroscopy, fluorescence titration, fluorescence microscopy, MS, UV/vis, circular dichroism (CD) and/or thermal denaturation temperature. A specific subset of techniques is often chosen to support a mechanistic theory for a specific biomolecular target and it is complicated by the qualitative nature of some. For complexes **2a-d**, the reported thermal denaturation temperatures (11, 6, 4 and 6 °C, respectively) showed **2a** to be the most effective DNA intercalator while **2d** caused the largest distortion of circular dichroism spectra and was more cytotoxic against HT-29 and MCF-7 cell lines [42].

The dual mode of action whereby the complexes coordinatively bind to the nucleobases of DNA after hydrolysation of the metal-Cl bond and intercalation was evidenced for all complexes except **13a-h** and **18** [1,38,40,42,50]. For complexes **13a-h** and **18** the respective accumulation of the complexes in the lysosomes and mitochondria of the cancer cells instead of interaction with DNA was considered [39,40]. This is discussed as part of the section on luminescence, as the techniques relied on the photophysical properties of the complexes.

In Table 7 the binding constants, as reported by Streciwilk *et al.* [1,50] are summarised. Fig. 8 depicts a metal-DNA adduct that formed when complexes **3b**, **3e**, **3f**, **4b**, **4f** and **10b** were

reacted with the nucleobase 9-ethylguanine [1,38,50]. Binding constants were determined using UV/vis, CD or fluorescence titration data while the presence of the metal-DNA adduct was confirmed with MS. From the binding constants it is apparent that the Rh(I)-complex **3b** bonds much stronger to calf-thymus DNA than the Ru(II)-complex **4b**, while complexes **3e**, **3f** and **4f** bonded to quadruplex c-Kit2 stronger than to ds26 [1,50].

Table 7
Binding constants for bonding of complexes with different oligodeoxyribonucleotides.

Complex	Binding constant[a] (M^{-1})		
	ct-DNA	ds26[d]	c-Kit2[d]
3b	80 (± 9.0)[b]	n.d.	n.d.
	40 (± 5.0)[c]	n.d.	n.d.
4b	5.4 (± 0.4)[b]	n.d.	n.d.
3e	n.d.	3.4 (± 0.4)	23 (± 7.0)
3f	n.d.	17 (± 3.0)	57 (± 9.0)
4f	n.d.	10 (± 1.0)	16 (± 1.0)

[a] x 10^3
[b] Determined from UV/vis DNA titrations
[c] Calculated from CD spectra
[d] Determined from fluorescence titrations
n.d. = not determined

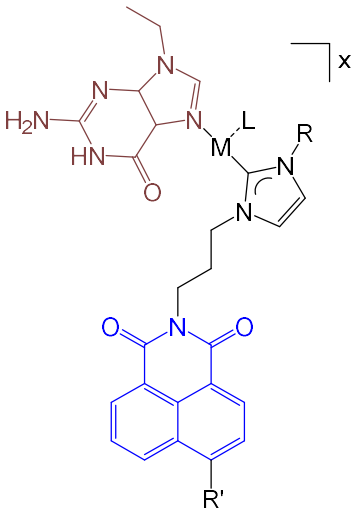

Fig. 8. Metal-DNA adduct that formed when **3b**, **3d**, **3f**, (Rh(I), x = +1, L = COD) **4b**, **4f** (Ru(II), x = +2, L = *p*-cymene) and **10b** (Rh(I), x = +1, L = COD) were reacted with 9-ethylguanine.

In experiments where complexes **3e**, **3f** and **4f** were reacted with 9-ethylguanine, the formation of G-tetrads, the building blocks of quadruplex DNA, was observed [1]. Together with the lack of changes in the CD spectra, it was suggested that when complexes **3e**, **3f** and **4f** bind to 9-ethylguanine of quadruplex c-Kit2, the conformation is stabilised and not disturbed, which points to a different anticancer mechanism [1]. A very detailed subsequent study, which focused on colorectal HCT116 cells, illustrated how the roles of p38 signalling and cell cycle regulation were responsible for the cytotoxicity of complexes **3f** and **4f**, more so than binding to DNA [43]. Complexes **3f** and **4f** were observed by fluorescence microscopy to accumulate in mitochondria. The highly oxidised mitochondrial membrane redox potential (MMRP) for **4f** corroborated the observed high levels of produced mitochondrial reactive oxygen species (mtROS) [43]. A consequent decrease in Bcl-xL levels was also observed while Bad protein levels were increased [43]. MtROS were observed to result in the activation of *in vitro* pro-apoptotic p38 mitogen-activated protein kinases (MAPK) signalling, in both HCT116 and MCF-7 cells, as it led to elevated antibody (pp 38 MAPK; T180/Y182) levels and ultimately, to G1 phase arrest. This was most prominent for **3f** [43]. The role of p38 signalling in causing cell death was confirmed after knock-down of p38*a* (MAPK14) and in the presence of chemical inhibitors, which led to an increase in cellular survival [43]. Interestingly, the role of p38 signalling as tumorigenic factor in triple negative breast cancers such as MDA-MB-231 was also discussed [43]. Immunoblotting, flow cytometric analysis and terminal deoxynucleotidyl transferase dUTP nick end labelling (TUNEL) assay, among others, were the techniques used [43].

Additional studies on the possible effects of complex **2d** on cellular metabolism using a metabolic sensor chip analysis system showed that respiration, extracellular acidification and cell impedance were influenced [42]. Complex **3b** was also shown to act *via* the mitochondrial pathway by influencing the mitochondrial membrane potential, determined by flow cytometric analysis and confirmed when moderately impeded by the protein BcI-2 [50].

3.3. Luminescence

Photoluminescence, or the re-emission of radiation from electronically/vibrationally excited states, is commonly described as *fluorescence* or, if the spin multiplicity changes and an intermediate state occurs, *phosphorescence* – normally, with respective nanosecond and microsecond excited-state lifetimes [76]. The part of the molecule that absorbs light and is

therefore responsible for the colour of the molecule is called a *chromophore*, in this case the 1,8-naphthalimide moiety. Phosphors or fluorophores (luminophores) are compounds or complexes exhibiting luminescence, albeit with a difference in the nature of the excited state [76,77].

Most of, if not all, organic phosphors and chromophores have π-electrons that form part of unsaturated, conjugated aromatic rings that, when bonded to metals, especially those in low oxidation states, may act as π-acceptors that cause the HOMO-LUMO gap to increase and permit re-emission of absorbed photons [78]. 2,2'-Bipyridine- (bipy) and terpyridine- (tpy) containing ruthenium complexes are well-known examples of inorganic/organometallic phosphors, of which $[Ru(bipy)_3]^{2+}$ provides somewhat of a benchmark to assess the performance of electrochemiluminescence emission [79]. Cyclometallated NHC complexes promote photoluminescence, with the added influence of the large σ-donor ability of the carbene carbon that increases the HOMO-LUMO gap even further [79]. Photoluminescence of NHC complexes has been observed for metals of groups 7-11 (Re, Ru, Os, Rh, Ir, Ni, Pd, Pt, Cu, Ag and Au), as recently reported by Visbal and Gimeno [79]. Photoluminescent complexes, especially containing NHC ligands, of earth abundant metals like Fe(II) and Cr(III) are still rare [80]. In addition to complexes with chelating ligands, NHC complexes may also be photoluminescent if they contain an attached chromophore and/or when metal-metal interactions are allowed, but these are less common [79].

The attraction of using 1,8-naphthalimide derivatives as a building block in the design of chemosensors is twofold: these compounds are quite easy to synthesise, while their photophysical properties can be greatly diversified by slight design modifications [81]. 1,8-Naphthalimide and N-methyl-1,8-naphthalimide exhibit weak fluorescence in the range 340-460 nm [81]. The lowest excited state is predominantly π-π* in character and fast intersystem crossing (ISC) from the excited π-π* singlet state to a close-lying n-π* triplet state is particularly efficient [82]. Introducing a halide at position 4 has a small effect on the photophysical properties, showing a bathofluoric shift of *ca*. 13 nm [81]. However, changing the halo substituent for an amino group has a marked effect on the emission, which induced a red shift (at *ca*. 540 nm), displaying green-coloured fluorescence while fluorescence intensity was increased [83]. This red shift is mimicked by introducing a heterocyclic moiety into the molecule at the 4-position [81]. By contrast, introducing an imidazole moiety at the N-position decreased the emission maximum to 375 nm [84]. Emission maxima of 420 and 440 nm were

obtained for the proligands of **21** and **22** of this study [46], while that of N-(3-imidazol-1-yl-propyl)-1,8-naphthalimide was reported as 461 nm [85].

Fluorescent complexes containing N-(3-imidazol-1-yl-propyl)-1,8-naphthalimide, similar to the complexes covered in this review, were studied by Nath and Baruah [85]. These complexes were however bonded to either a Mn(II), Co(II), Zn(II), Cd(II) or Hg(II) centre *via* the imidazole N-atom [85]. The influence of the metal, the method of measurement (solid state or in solution) and the temperature on the conformation and subsequently on the fluorescence properties was investigated [85]. The three possible conformations, shown in Fig. 9, affected the photo-electron transfer (PET) or intramolecular charge transfer (ICT) mechanism of the complexes [85]. Quantum yields of the complexes were enhanced compared to that of the ligand. The nature of co-ligands (Cl, *ca.* 420-430 nm *vs.* SCN, *ca.* 475 nm) affected the emission wavelengths of the complexes relative to that of the ligand (461 nm). It was concluded that an intramolecular charge-transfer (ICT) process was able to stabilise the ground state, which led to emissions at lower wavelengths, while geometries with π-stacking of 1,8-naphthalimides showed emissions at long wavelengths [85].

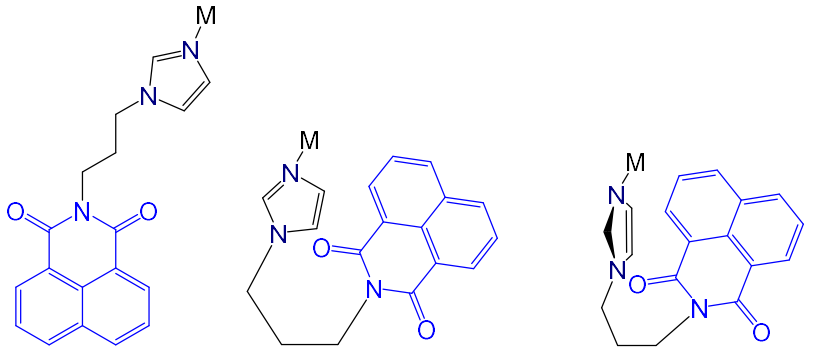

Fig. 9. Possible conformations of N-bonded Mn(II), Co(II), Zn(II), Cd(II) and Hg(II) complexes containing an 1,8-naphthalimide moiety tethered to an imidazole ring.

Currently, the main applications of photoluminescent NHC complexes are Ir(III)-based dopants for organic light emitting diode (OLED) devices that emit single-colour or white light as well as Ru(II)-based dye-sensitised solar cells (DSSCs) [79]. Parameters that are commonly studied in the context of photophysical properties include the absorption/emission wavelength, Stokes shift, excited state lifetime (τ), quantum yield (Φ) and radiative rate constant (k_r).

Table 8
Photophysical properties of photoluminescent complexes and precursor azolium salts measured at room temperature.

Complex	Metal	λ_{em} (nm)[a]	Φ (%)[b,c]	τ (ns)[d]	k_r (s^{-1})	Solvent	λ_{em} (nm)[g]	Ref
13a	Au(I)	507	2	7.8 (45%), <1.0 (55%)	n.d.	Aerated acetone	504 (4, 7.3)	[39]
13b		487	9	7.2 (78%), 2.8 (22%)	n.d.		507 (28, 8.7)	
13c		500	1	1.1 (76%), <1.0 (24%)	n.d.		502 (4, 9.1)	
13d		504	1	6.9 (33%), <1.0 (67%)	n.d.		503 (4, 7.2)	
13f		503	2	8.3 (82%), 2.6 (18%)	n.d.		504 (17, 8.4)	
13g		499	1	4.3 (9%), 1.0 (91%)	n.d.		501 (5, 4.7)	
13h		504	8	<1.0	n.d.		503 (12, 9.0)	
13i		451	1	n.d.	n.d.	De-aerated DCM	410, 430 (0.21, n.d.)	[41]
14	Cu(I)	426	8	n.d.	n.d.			
16a	Rh(I)	438, 462, 505 (441)	0.14	9.9	n.d.	Aerated acetone	433 (1.78, n.d.)	[44]
16b		504	1.0	8.7	n.d.		502 (74.5, 9.6)	
17a	Ir(I)	458 (447)	0.45	7.7	n.d.		433 (1.78, n.d.)	
17b		506	0.9	8.7	n.d.		502 (74.5, 9.6)	
19	Cu(I)	428	22	n.d.	n.d.	De-aerated DCM	406, 424 (0.73, n.d.)	[38]
20	Au(I)	429	32	n.d.	n.d.			
21a	Ir(III)	670	1.5	0.78 x 10^3	1.92 × 10^4	De-aerated DCM	420 [h] (21, 3.1)	[46]
			1.1	0.66 x 10^3	1.67 × 10^4	De-aerated CH_3CN		
		655[f]	n.d.	12.6 x 10^3 [f]	n.d.	DCM:MeOH (1:1)		
		648	(0.18)[e]	(8.0 x 10^3)	n.d.	Polymeric film		[45]

21b	645	17.5	17.5 x 10^3	1.00 × 10^4	De-aerated DCM	420 [h] (21, 3.1)	[46]
		12.0	14.7 x 10^3	0.82 × 10^4	De-aerated CH_3CN		
	640[f]	n.d.	21.5 x 10^3 [f]	n.d.	DCM:MeOH (1:1)		
	631	(0.22)[e]	(13.7 x 10^3)	n.d.	Polymeric film		[45]
21c	665	4.3	2.2 x 10^3	1.95 × 10^4	De-aerated DCM	420 [h] (21, 3.1)	[46]
		3.2	2.2 x 10^3	1.45 × 10^4	De-aerated CH_3CN		
	655[f]	n.d.	13.8 x 10^3 [f]	n.d.	DCM:MeOH (1:1)		
	641	(0.16)[e]	(8.6 x 10^3)	n.d.	Polymeric film		[45]
22a	690	4.4	6.7 x 10^3	0.66 × 10^4	De-aerated DCM	440 [h] (61, 5.6)	[46]
		3.6	6.3 x 10^3	0.57 × 10^4	De-aerated CH_3CN		
	665[f]	n.d.	21.3 x 10^3 [f]	n.d.	DCM:MeOH (1:1)		
22b	660	11.5	26.4 x 10^3	0.44 × 10^4	De-aerated DCM	440 [h] (61, 5.6)	
		9.1	22.7 x 10^3	0.40 × 10^4	De-aerated CH_3CN		
	645[f]	n.d.	38.6 x 10^3 [f]	n.d.	DCM:MeOH (1:1)		
22c	680	6.6	10.3 x 10^3	0.64 × 10^4	De-aerated DCM	440 [h] (61, 5.6)	
		5.3	9.4 x 10^3	0.56 × 104	De-aerated CH_3CN		
	660[f]	n.d.	23.8 x 10^3 [f]	n.d.	DCM:MeOH (1:1)		

[a] λ_{ex} **13a–h**, **13i**, **14**, **16-17**, **19**, **20**: 405 nm, 340 nm, 340 nm, 405 (340) nm, 350 nm, 350 nm
[b] λ_{ex} **16-17**, **21a–c**: 405 nm, (420) nm
[c] Solution ref for **13a–h**; **13i**, **14**, **19**, **20**; **21a–c–22**: $[Ru(bipy)_3](PF_6)_2$ in aerated MeCN; 9,10-diphenylanthracene in cyclohexane; $[Ru(bipy)_3]Cl_2$ in air-equilibrated water.
[d] λ_{ex} **13a–h**, **16-17**, **21**: 372 nm, 405 nm, (465) nm
[e] Raw Φ values, not as percentages
[f] Temperature: -196.15 °C
[g] Data for azolium salt; Values in brackets represent Φ (%) and τ (ns)

[h] Data for the proligand before azolium salt formation in de-aerated DCM
n.d. = not determined

The introduction of the naphthalimide moiety into the NHC scaffold changed the lowest excited energy state of the complexes. All of the complexes predominantly emit from intramolecular charge transfer (ICT) bands since the lowest energy transition occurs from the NHC-centred HOMO to the naphthalimide-centred LUMO (Fig. 10) [39,41,45,46]. For this series of complexes, the influence of structural features in the NHC-naphthalimide moiety *i.e.* π-conjugation and electron-withdrawing groups, as well as cyclometallation and measurement conditions (*i.e.* temperature and physical state) are discussed [86].

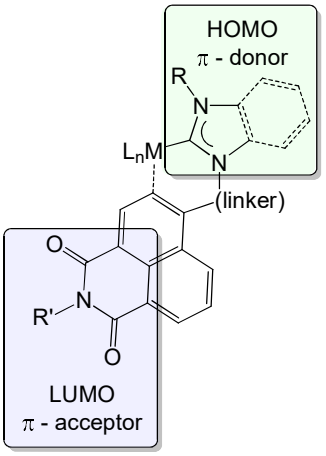

Fig. 10. Origin of ICT showing the centred position of the HOMO and LUMO on the complexes.

Perhaps the most noteworthy detail reflected is that emission data from most of the metal complexes of this study (**8a-d**, **13a-i**, **14**, **17** and **18**) exhibit fluorescence lifetimes (Table 8). Only the Ir(III) complexes **19a-c** and **20a-c** have phosphorescence decay lifetimes (0.78-38.6 μs).

Au(I), Rh(I) and Ir(I) complexes **13a-h**, **16** and **17** emitted in the blue to blue-green region with fluorescence lifetimes and relatively low quantum yields [39]. Models of the HOMOs and LUMOs revealed that the N-appended phenyl group of complex **13d** acted as a donor that promoted π-conjugation, resulting in its emission being red-shifted and extending its excited state lifetime relative to **13c**, which had an ethyl tether [39]. Complexes **13i**, **14**, **19** and **20**

emitted in the blue region, with **19** and **20** having high quantum yields, attributed to the presence of the phenyl ethynyl linker that also promoted π-conjugation [41]. A blue shift is also observed for Cu(I) complexes **14** and **19** relative to Au(I) complexes **13i** and **20** [41]. Metal-related quenching was less prominent for complexes **16b** and **17b** which had higher quantum yields than **16a** and **17a**, respectively [44]. Complexes **16b** and **17b** were consequently chosen for further studies on confocal microscopy (*vide infra*) [44]. The larger relative emission intensities of **16b** and **17b** were attributed to the longer electron-donating amine tether which placed the naphthalimide moiety further away from the metal [44]. The emission wavelengths observed for **16a** at 438 nm and 462 nm, when excited at 405 nm, was ascribed to one of the rotamers and emission at 505 nm to the other [44].

Cyclometallation of the naphthalimide moiety resulted in spin-orbit coupling that caused metal d-orbitals to contribute slightly to previously ligand centred (LC) emissions by energetically allowing marginal metal-to-ligand charge transfer (MLCT) [45,46]. Complexes **21a-c** and **22a-c** emit in the red region due to the contribution from d-orbitals, which increased the energy of the HOMO and shifted the resulting absorption above 400 nm [45,46]. The radiative rate constants are, however, still indicative of mainly LC emission [45,46]. Benzimidazolylidene derivatives (complexes **22a-c**) promoted π-conjugation in the imidazolylidene ring that consequently red shifted the emissions of the complexes relative to **21a-c**, in addition to increasing excited state lifetimes and decreasing radiative rate constants, which mostly resulted in larger quantum yields [46]. A marginal contribution from metal d-orbitals was also observed for complexes **16a** and **17a** [44].

In the archetypal complex $[Ir(ppy)_2(bpy)]^+$, phosphorescence is ascribed to either ^{3}LC or ^{3}MLCT transition states [87], which led to the general belief that the excited state is a mix of these two states [88]. Having combined MLCT and LC character was also realised for a heteroleptic Ir(III) complex containing a naphthalene-type cyclometallated moiety (Fig. 11), with R = diphenylamine [89]. However, if R = H, LC emission dominated [89]. Both complexes emitted in the red-to-near-infrared region [89]. Lanoë *et al.* confirmed with time-dependent DFT calculations that the presence of the naphthalimide chromophore in complexes **21a-c** and **22a-c** had a dramatic effect on the nature of the excited states, which now exhibited mainly naphthalimide-centred ^{3}LC character [46].

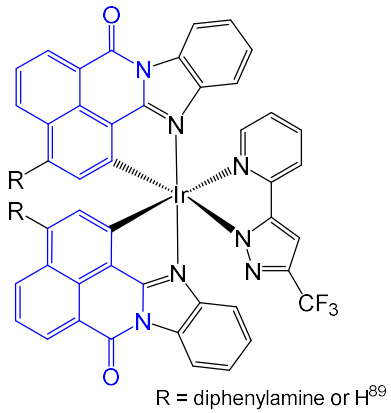

Fig. 11. Naphthalene-type cyclometallated Ir(III) complexes, emitting in the red-to-near-infrared region.

The influence of ancillary ligands is realised when considering complexes **21b** and **22b** which contain electron-withdrawing fluorine atoms [45,46]. Relative to the complexes within their respective series (**21a-c** and **22a-c**), their emissions are blue-shifted in addition to having the longest excited state lifetimes and largest quantum yields as well as lowest radiative rate constants [45,46]. In complexes **21b** and **22b** the HOMO is stabilised and MLCT contribution minimal [45,46]. Temperature and physical state are important factors that influence photophysical properties dramatically and are often difficult to replicate computationally [39]. Complexes that were evaluated at -196 °C (**21-22a-c**) had emissions that were blue-shifted compared to when they were assessed at room temperature in solution [45,46]. When the complexes were evaluated as polymeric films (**21a-c**) that contain poly(bisphenol A carbonate) and 0.5 w% of the complex, emissions were blue-shifted and had longer excited state lifetimes compared to when they were assessed in solution [45,46].

One should take caution when comparing quantum yields for complexes studied by the various authors, as different reference standards (Table 8) were used to compute percentages. For **21a-c**, measured as a polymeric film, raw values without the reference were given [90]. It is, however, apparent that when free azolium salts were coordinated to the respective metals as (benz)imidazole(in)ylidene ligands, quantum yields decreased and photoluminescence was quenched by introduction of a heavy atom. For complexes **16** and **17** quenching was attributed to PET [44]. Similar quenching was observed for **2a**, **3b** and **4b**, which prevented the study of their photophysical properties and application in fluorescence microscopy during mechanistic studies of their anticancer activity [42,50].

Complexes **3e**, **3f**, **4f** and **10b** had higher quantum yields owing to the ethylthio-substituent [1] at the *para*-position of the naphthalene ring as well as the bis-naphthalimide structure [38]. The complexes emitted in the blue region and were used to investigate cellular uptake using fluorescence microscopy [1,38]. Their photophysical properties were also utilised in DNA fluorescence titrations and during a fluorescence resonance energy transfer (FRET) melting assay, as mentioned before [1].

For complex **13c** confocal fluorescence microscopy was performed with MCF-7 cells [39]. Emission at 500-550 nm showed rapid uptake at concentration values well-below IC_{50} values and spheroidal localisation in the cytoplasm, with **13c** co-localising with commercial fluorophores in the lysosome [39]. Subsequently, fluorescence lifetime imaging microscopy (FLIM) showed a longer excited state lifetime for **13c** which was closer to that of the free azolium salt. This is an indication that **13c** probably dissociates in a biological environment or when exposed to photons in such an environment [39]. Confocal fluorescence microscopy was also used to confirm the mitochondrial accumulation of complex **18** and **18**-BSA [40]. Pearson's correlation coefficient was used to illustrate positive co-localisation of complexes **16b** or **17b** and an additional marker in the endoplasmic reticulum, mitochondria, and the lysosome of either HT-29 (colon) or PT-45 (pancreatic) cancer cells [44]. Co-localisation was observed to occur most prominently in the endoplasmic reticulum for both cells lines, with **16b** and **17b** behaving similarly [44]. The ability to observe the interactions and localisation of these complexes in cells paves the way to better understand their cytotoxic mechanism.

4. Outlook and Conclusion

In this review, the progress that has been made with regards to naphthalimide-NHC ligand scaffolds has been highlighted. The recent tendency to apply compounds and materials as multi-functional agents in different applications has been shown herein. Metal complexes with naphthalimide-containing NHC ligands are interesting molecular targets, readily synthesised by common silver transmetallation (for Rh(I), Ru(II), Ir(I), Ir(III), Au(I) and Cu(I)) or by direct reaction with metal precursors in the presence of a base (for Au(I), Ag(I), Ir(I), Pd(II) and Pt(II)). Synthesis by post-synthetic modification of the ligand after metal coordination has also been reported. The synthesis of the respective azolium salts was realised by functionalisation of (benz)imidazole or imidazolium through condensation, substitution or by means of ring-

building. Some of the complexes adapted interesting conformations and were present as pairs of stable enantiomers.

The complexes effectively catalysed Larock heteroannulation and Suzuki-Miyaura cross-coupling reactions, with high respective product yields of 82% and 95%. A wide substrate scope and the influence of π-π stacking interactions were highlighted for the Larock heteroannulation reaction. These limited examples point out that catalytic applications of naphthalimide-NHC complexes remain relatively unexplored. Evaluation of the anticancer, antibacterial and fungicidal properties of the studied complexes were presented. Rh(I) complexes were shown to be more cytotoxic than Ru(II) analogues but those with bis-naphthalimide and bis-NHC moieties showed superior cytotoxic properties. Rh(I) and Ru(II) complexes also exhibited appreciable activity against gram-positive bacteria. The roles of lipophilicity and steric hindrance, in relation to the anticancer, antibacterial and fungicidal properties of the complexes, were emphasised. Among these complexes, mechanistic studies revealed that complexes showed a preference for quadruplex DNA, binding coordinatively and *via* intercalation. Some of the complexes were also shown to effectively target TrxR, accumulate in cells' mitochondria, lysosomes or the endoplasmic reticulum and/or act *via* p38 signalling to induce cell death.

Many of the complexes were photoluminescent, emitting predominantly from ICT bands in red, blue-green or blue regions with either phosphorescence or fluorescence lifetimes. The influence of π-conjugation as well as ancillary ligands with fluorine atoms were particularly illustrated. These complexes are examples of metal NHCs that owe their photophysical properties to the presence of a naphthalimide chromophore embedded within the NHC ligand [91]. Studies combining biological and luminescent application fields in specialised confocal fluorescence microscopy and fluorescence lifetime imaging microscopy (FLIM) experiments, were used to elucidate anticancer mechanisms.

This class of compounds, transition metal naphthalimide-containing NHC complexes, could be an epicentre for future work as it covers many prevalent topics in the synthesis and characterisation of metal NHCs. Complexes with the naphthalimide moiety present in the NHC backbone are underrepresented, as are those with varied naphthalimide-tether lengths, bis-NHCs, abnormally coordinated NHCs, other NHC scaffolds such as triazolylidene or cyclic alkyl amino carbenes (CAAC) as well as those containing earth abundant metals. This class of

metal complexes can also be expanded by consideration of similar pairings of the NHC moiety with analogues of 1,8-naphthalimide (e.g. phthalimide, 1,2-naphthalimide, 2,3-naphthalimide, phenanthrene-9,10-dicarboximide and biphenyl-2,2'-dicarboximide). Finally, integration of the photophysical and biological or catalytic properties for photodynamic therapy, photoredox catalysis and photocatalysis is still unexplored for this class of compounds. This presents exciting avenues for future studies which will enable one to fully benefit from multi-functional naphthalimide-tagged metal-NHC complexes.

Conflicts of interest

There are no conflicts to declare.

Acknowledgements

This work is based on the research supported by the National Research Foundation of South Africa (Grant Numbers: LR 122836, FPM Grant No. 117995 and ML 120840) and the University of Pretoria.

5. References

[1] W. Streciwilk, A. Terenzi, X. Cheng, L. Hager, Y. Dabiri, P. Prochnow, J.E. Bandow, S. Wölfl, B.K. Keppler, I. Ott, Eur. J. Med. Chem., 156 (2018) 148-161.
[2] Y. Sun, S. Wei, Y. Zhao, X. Hu, J. Fan, J. Lumin., 132 (2012) 879-886.
[3] M.P. Singh, A. Tarai, J.B. Baruah, ChemistrySelect, 3 (2018) 6364-6373.
[4] A. Kamal, N.R. Bolla, P.S. Srikanth, A.K. Srivastava, Expert Opinion on Therapeutic Patents, 23 (2013) 299-317.
[5] S. Stoyanov, P. Petrov, M. Stoyanova, M. Dangalov, B. Shivachev, R. Nikolova, I. Petkov, J. Photochem. Photobiol. A, 250 (2012) 92-98.
[6] C. Geraghty, C. Wynne, R.B.P. Elmes, Coord. Chem. Rev., 437 (2021) 213713.
[7] R.M. Duke, E.B. Veale, F.M. Pfeffer, P.E. Kruger, T. Gunnlaugsson, Chem. Soc. Rev., 39 (2010) 3936-3953.
[8] J. Qian, G. Zhang, J. Cui, L. Zhou, Z. Chen, Z. Zhang, W. Zhang, Sens. Actuators, B Chem., 311 (2020) 127923.
[9] B. Carlotti, M. Poddar, F. Elisei, A. Spalletti, R. Misra, J. Phys. Chem. C, 123 (2019) 24362-24374.
[10] Y. Liu, D. Lee, X. Zhang, J. Yoon, Dyes Pigm., 139 (2017) 658-663.
[11] G.L.V. Damu, Q. Wang, H. Zhang, Y. Zhang, J. Lv, C. Zhou, Sci. China Chem., 56 (2013) 952-969.
[12] Y.-L. Luo, K. Baathulaa, V.K. Kannekanti, C.-H. Zhou, G.-X. Cai, Sci. China Chem., 58 (2015) 483-494.
[13] F. Li, J. Cui, L. Guo, X. Qian, W. Ren, K. Wang, F. Liu, Bioorg. Med. Chem., 15 (2007) 5114-5121.

[14] M. Dangalov, S. Yordanova, M. Stoyanova, D. Cheshmedzhieva, P. Petrov, S. Stoyanov, J. Mol. Struct., 1125 (2016) 705-713.
[15] C. Rizzo, P. Cancemi, L. Mattiello, S. Marullo, F. D'Anna, ACS Appl. Mater. Interfaces, 12 (2020) 48442-48457.
[16] K.P. McDonald, R.O. Ramabhadran, S. Lee, K. Raghavachari, A.H. Flood, Org. Lett., 13 (2011) 6260-6263.
[17] W. Ma, S. Zhang, Z. Tian, Z. Xu, Y. Zhang, X. Xia, X. Chen, Z. Liu, Eur. J. Med. Chem., 181 (2019) 111599.
[18] V.M. Chernyshev, E.A. Denisova, D.B. Eremin, V.P. Ananikov, Chem. Sci., 11 (2020) 6957-6977.
[19] J. Cheng, L. Wang, P. Wang, L. Deng, Chem. Rev., 118 (2018) 9930-9987.
[20] E. Peris, Chem. Rev., 118 (2018) 9988-10031.
[21] S. Karthik, T. Gandhi, Org. Lett., 19 (2017) 5486-5489.
[22] L. Mercs, M. Albrecht, Chem. Soc. Rev., 39 (2010) 1903-1912.
[23] M.D. Tomczyk, K.Z. Walczak, Eur. J. Med. Chem., 159 (2018) 393-422.
[24] R. Tandon, V. Luxami, H. Kaur, N. Tandon, K. Paul, Chem. Rec., 17 (2017) 956-993.
[25] M. Porchia, M. Pellei, M. Marinelli, F. Tisato, F. Del Bello, C. Santini, Eur. J. Med. Chem., 146 (2018) 709-746.
[26] M. Zaki, S. Hairat, E.S. Aazam, RSC Adv., 9 (2019) 3239-3278.
[27] A. Bonfiglio, M. Mauro, Eur. J. Inorg. Chem., 2020 (2020) 3427-3442.
[28] T. Gunnlaugsson, M. Glynn, G.M. Tocci, P.E. Kruger, F.M. Pfeffer, Coord. Chem. Rev., 250 (2006) 3094-3117.
[29] R. Wang, X. Li, J. Yoon, ACS Appl. Mater. Interfaces, 13 (2021) 19543-19571.
[30] Á. Vivancos, C. Segarra, M. Albrecht, Chem. Rev., 118 (2018) 9493-9586.
[31] N.U.D. Reshi, J.K. Bera, Coord. Chem. Rev., 422 (2020) 213334.
[32] P.K.R. Panyam, T. Gandhi, Adv. Synth. Catal., 359 (2017) 1144-1151.
[33] P.K.R. Panyam, R. Sreedharan, T. Gandhi, Org. Biomol. Chem., 16 (2018) 4357-4364.
[34] M. Dangalov, M. Stoyanova, P. Petrov, M. Putala, N.G. Vassilev, J. Organomet. Chem., 817 (2016) 1-14.
[35] M. Dangalov, P. Petrov, N. Vassilev, Bulg. Chem. Commun., 49 (2017) 42-49.
[36] M. Dangalov, P. Petrov, N.G. Vassilev, J. Mol. Struct., 1230 (2021) 129944.
[37] M. Dangalov, P. Petrov, N.G. Vassilev, J. Organomet. Chem., 824 (2016) 104-117.
[38] W. Streciwilk, A. Terenzi, F. Lo Nardo, P. Prochnow, J.E. Bandow, B.K. Keppler, I. Ott, Eur. J. Inorg. Chem., 2018 (2018) 3104-3112.
[39] L.M. Groves, C.F. Williams, A.J. Hayes, B.D. Ward, M.D. Isaacs, N.O. Symonds, D. Lloyd, P.N. Horton, S.J. Coles, S.J.A. Pope, Dalton Trans., 48 (2019) 1599-1612.
[40] S. Sen, M.W. Perrin, A.C. Sedgwick, E.Y. Dunsky, V.M. Lynch, X.-P. He, J.L. Sessler, J.F. Arambula, Chem. Commun., 56 (2020) 7877-7880.
[41] P.-H. Lanoë, B. Najjari, F. Hallez, G. Gontard, H. Amouri, Inorganics, 5 (2017) 58.
[42] A. Meyer, L. Oehninger, Y. Geldmacher, H. Alborzinia, S. Wolfl, W.S. Sheldrick, I. Ott, ChemMedChem, 9 (2014) 1794-1800.
[43] Y.S. Dabiri, A.; Theobald, J.; Blagojevic, B.; Streciwilk, W.; Ott, I.; Wölfl, S.; Cheng, X. , Int. J. Mol. Sci., 19 (2018) 3964.
[44] I.M. Daubit, S. Wortmann, D. Siegmund, S. Hahn, P. Nuernberger, N. Metzler-Nolte, Chem. Eur. J., 27 (2021) 6783-6794.
[45] P.-H. Lanoë, J. Chan, G. Gontard, F. Monti, N. Armaroli, A. Barbieri, H. Amouri, Eur. J. Inorg. Chem., 2016 (2016) 1631-1634.
[46] P.-H. Lanoë, J. Chan, A. Groué, G. Gontard, A. Jutand, M.-N. Rager, N. Armaroli, F. Monti, A. Barbieri, H. Amouri, Dalton Trans., 47 (2018) 3440-3451.

[47] A. Groué, J.-P. Tranchier, M.-N. Rager, G. Gontard, M. Jean, N. Vanthuyne, H.R. Pearce, A.L. Cooksy, H. Amouri, Inorg, 58 (2019) 2930-2933.
[48] C.L. Fleming, T.D. Ashton, F.M. Pfeffer, Dyes Pigm., 109 (2014) 135-143.
[49] H. Yu, M. Fu, Y. Xiao, Phys. Chem. Chem. Phys., 12 (2010) 7386-7391.
[50] W. Streciwilk, A. Terenzi, R. Misgeld, C. Frias, P.G. Jones, A. Prokop, B.K. Keppler, I. Ott, ChemMedChem, 12 (2017) 214-225.
[51] L. Zhu, L. Cheng, Y. Zhang, R. Xie, J. You, The Journal of Organic Chemistry, 72 (2007) 2737-2743.
[52] S. Sen, Y. Li, V. Lynch, K. Arumugam, J.L. Sessler, J.F. Arambula, Chem. Commun., 55 (2019) 10627-10630.
[53] F. Nahra, S.R. Patrick, A. Collado-Martinez, S.P. Nolan, Polyhedron, 84 (2014) 59-62.
[54] S. Prühs, C.W. Lehmann, A. Fürstner, Organometallics, 23 (2004) 280-287.
[55] Y. Tatsuno, T. Yoshida, S. Otsuka, N. Al-Salem, B.L. Shaw, Inorg. Synth., 28 (1990) 342-345.
[56] P. Barbaro, P.S. Pregosin, R. Salzmann, A. Albinati, R. Kunz, Organometallics, 14 (1995) 5160-5170.
[57] D.J. Mabbott, B.E. Mann, P.M. Maitlis, Journal of the Chemical Society, Dalton Transactions, (1977) 294-299.
[58] H. Jacobsen, A. Correa, A. Poater, C. Costabile, L. Cavallo, Coord. Chem. Rev., 253 (2009) 687-703.
[59] R. Hamze, S. Shi, S.C. Kapper, D.S. Muthiah Ravinson, L. Estergreen, M.-C. Jung, A.C. Tadle, R. Haiges, P.I. Djurovich, J.L. Peltier, R. Jazzar, G. Bertrand, S.E. Bradforth, M.E. Thompson, J. Am. Chem. Soc., 141 (2019) 8616-8626.
[60] H.V. Huynh, Y. Han, R. Jothibasu, J.A. Yang, Organometallics, 28 (2009) 5395-5404.
[61] L. Oehninger, R. Rubbiani, I. Ott, Dalton Trans., 42 (2013) 3269-3284.
[62] A. Frei, Antibiotics, 9(2) (2020).
[63] S.K. Singh, D.S. Pandey, RSC Adv., 4 (2014) 1819-1840.
[64] T. Onodera, I. Momose, M. Kawada, Chemical and Pharmaceutical Bulletin, 67 (2019) 186-191.
[65] C.P. Bagowski, Y. You, H. Scheffler, D.H. Vlecken, D.J. Schmitz, I. Ott, Dalton Trans., (2009) 10799-10805.
[66] R.D. Wells, Trends in Biochemical Sciences, 32 (2007) 271-278.
[67] Ö. Karaca, S.M. Meier-Menches, A. Casini, F.E. Kühn, Chem. Commun., 53 (2017) 8249-8260.
[68] D.L. Vaux, Biochimica et biophysica acta, 1813 (2011) 546-550.
[69] K.J. Kilpin, C.M. Clavel, F. Edafe, P.J. Dyson, Organometallics, 31 (2012) 7031-7039.
[70] S. Schäfer, I. Ott, R. Gust, W.S. Sheldrick, Eur. J. Inorg. Chem., 2007 (2007) 3034-3046.
[71] S.J. Patankar, P.C. Jurs, Journal of Chemical Information and Computer Sciences, 40 (2000) 706-723.
[72] J.W. Hawkins, A. Dugaiczyk, Gene, 19 (1982) 55-58.
[73] H. Scheffler, Y. You, I. Ott, Polyhedron, 29 (2010) 66-69.
[74] C. O'Beirne, N.F. Alhamad, Q. Ma, H. Müller-Bunz, K. Kavanagh, G. Butler, X. Zhu, M. Tacke, Inorg. Chim. Acta, 486 (2019) 294-303.
[75] P.O. Asekunowo, R.A. Haque, M.R. Razali, Transition Metal Chemistry, 40 (2015) 79-88.
[76] B. Valeur, M.N. Berberan-Santos, Journal of Chemical Education, 88 (2011) 731-738.
[77] A. Mitra, Resonance, 24 (2019) 623.
[78] A. de Almeida, R. Bonsignore, Bioorg. Med. Chem. Lett., 30 (2020) 127219.
[79] R. Visbal, M.C. Gimeno, Chem. Soc. Rev., 43 (2014) 3551-3574.
[80] O.S. Wenger, J. Am. Chem. Soc., 140 (2018) 13522-13533.

[81] P.A. Panchenko, O.A. Fedorova, Y.V. Fedorov, Russ. Chem. Rev., 83 (2014) 155-182.
[82] T. Gerbich, H.-C. Schmitt, I. Fischer, R. Mitrić, J. Petersen, J. Phys. Chem. A, 120 (2016) 2089-2095.
[83] M.S. Alexiou, V. Tychopoulos, S. Ghorbanian, J.H.P. Tyman, R.G. Brown, P.I. Brittain, J. Chem. Soc., Perkin Trans. 2, (1990) 837-842.
[84] J. Wang, L. Yang, C. Hou, H. Cao, Org. Biomol. Chem., 10 (2012) 6271-6274.
[85] J.K. Nath, J.B. Baruah, Inorg. Chem. Front., 1 (2014) 342-351.
[86] S. Yoon, T.S. Teets, Chem. Commun., 57 (2021) 1975-1988.
[87] S.-H. Wu, J.-W. Ling, S.-H. Lai, M.-J. Huang, C.H. Cheng, I.C. Chen, J. Phys. Chem. A, 114 (2010) 10339-10344.
[88] S. Abbas, I.-u.-D. Din, A. Raheel, A. Tameez ud Din, Appl. Organomet. Chem., 34 (2020) e5413.
[89] P. Rajakannu, H.S. Kim, W. Lee, A. Kumar, M.H. Lee, S. Yoo, Inorg, 59 (2020) 12461-12470.
[90] A.M. Brouwer, Pure Appl. Chem., 83 (2011) 2213-2228.
[91] C. Hemmert, H. Gornitzka, Dalton Trans., 45 (2016) 440-447.